

Cyclin B3 promotes anaphase I onset in oocyte meiosis

Mehmet E Karasu, Nora Bouftas, Katja Wassmann, Scott Keeney

▶ **To cite this version:**

Mehmet E Karasu, Nora Bouftas, Katja Wassmann, Scott Keeney. Cyclin B3 promotes anaphase I onset in oocyte meiosis. Journal of Cell Biology, 2019, 218 (4), pp.1265-1281. 10.1083/jcb.201808091 . hal-02171206

HAL Id: hal-02171206

https://hal.sorbonne-universite.fr/hal-02171206

Submitted on 2 Jul 2019

HAL is a multi-disciplinary open access archive for the deposit and dissemination of scientific research documents, whether they are published or not. The documents may come from teaching and research institutions in France or abroad, or from public or private research centers.

L'archive ouverte pluridisciplinaire **HAL**, est destinée au dépôt et à la diffusion de documents scientifiques de niveau recherche, publiés ou non, émanant des établissements d'enseignement et de recherche français ou étrangers, des laboratoires publics ou privés.

Cyclin B3 promotes anaphase I onset in oocyte meiosis

Mehmet E. Karasu [1, 2, 3, 6], Nora Bouftas[4, 5, 6], Scott Keeney[1, 2, 3, *], and Katja Wassmann[4, 5, 7, *]

[1]Molecular Biology Program, Memorial Sloan Kettering Cancer Center, 1275 York Ave., New York, New York 10065, USA

[2]Louis V. Gerstner, Jr. Graduate School of Biomedical Sciences, Memorial Sloan Kettering Cancer Center, 1275 York Ave., New York, New York 10065

[3]Howard Hughes Medical Institute, Memorial Sloan Kettering Cancer Center, 1275 York Ave., New York, New York 10065

[4]Sorbonne Université, Institut de Biologie Paris Seine (IBPS), 7 Quai St. Bernard, Paris, 75005 France

[5]Sorbonne Université, CNRS UMR7622 Developmental Biology Lab, 7 Quai St. Bernard , 75005, Paris, France

[6]These authors contributed equally

[7]Lead Contact

*Corresponding authors: Katja Wassmann (katja.wassmann@upmc.fr)
ORCID: 0000-0001-5442-5192
Scott Keeney (s-keeney@ski.mskcc.org)
ORCID: 0000-0002-1283-6417

Short Title: Role of cyclin B3 in oocyte meiosis I

Abstract

Meiosis poses unique challenges because two rounds of chromosome segregation must be executed without intervening DNA replication. Mammalian cells express numerous, temporally regulated cyclins, but how these proteins collaborate to control meiosis remains poorly understood. Here we show that female mice genetically ablated for cyclin B3 are viable, indicating the protein is dispensable for mitotic divisions, but are sterile. Mutant oocytes appear normal until metaphase I but then display a highly penetrant failure to transition to anaphase I. They arrest with hallmarks of defective APC/C activation, including no separase activity, high CDK1 activity, and high cyclin B1 and securin levels. Partial APC/C activation occurs, however, as exogenously expressed APC/C substrates can be degraded. Cyclin B3 forms active kinase complexes with CDK1, and meiotic progression requires cyclin B3-associated kinase activity. Cyclin B3 homologs from frog, zebrafish, and fruitfly rescue meiotic progression in cyclin B3-deficient mouse oocytes, indicating conservation of the biochemical properties and possibly cellular functions of this germline-critical cyclin.

eToc Summary:

Cyclins control the switch-like cell cycle transitions that orchestrate orderly duplication and segregation of genomes. Karasu, Bouftas, et al. delineate an essential function for mouse cyclin B3 for anaphase onset in the first meiotic division of oocytes.

Keywords:

Oocytes, meiosis, cell division, anaphase promoting complex/cyclosome (APC/C), cyclin B3, *Ccnb3*, cyclin dependent kinase (CDK), metaphase-to-anaphase transition

Introduction

Eukaryotic cell division depends on oscillations of cyclin-dependent kinases (CDKs) associated with specific cyclins (Morgan, 1997; Malumbres et al., 2009; Uhlmann et al., 2011; Fisher et al., 2012). In vertebrate somatic cells, progression from G1 into S phase, G2, and mitosis depends on the cyclin D family, followed by the cyclin E, A, and B families (Morgan, 1997). Ordered CDK activity likewise governs progression through meiosis: chromosome condensation, congression, and alignment require a rise in cyclin B1-CDK1 activity, then anaphase onset is driven by inactivation of cyclin B1-CDK1 by the anaphase promoting complex/ cyclosome (APC/C), an E3 ubiquitin ligase that targets substrates for degradation (Heim et al., 2017). Cyclin B1-CDK1 activity then re-accumulates, without DNA replicating again while cyclin B1-CDK1 activity is low between meiosis I and II (Petronczki et al., 2003; El Yakoubi and Wassmann, 2017). Apart from cyclin B2 which can compensate for loss of cyclin B1 (Li et al., 2018a), the roles of specific cyclins in determining orderly meiotic progression remain poorly understood in mammalian oocytes.

Particularly enigmatic is cyclin B3, which forms a family distinct from other cyclins based on sequence alignments, but which contains structural motifs characteristic of both A- and B-type cyclins (Nieduszynski et al., 2002; Gunbin et al., 2011). Chicken cyclin B3 shows nuclear localization when ectopically expressed in HeLa cells, similar to A-type cyclins (Gallant and Nigg, 1994), but its orthologs cluster more closely with B-type cyclins based on amino acid sequence (Nieduszynski et al., 2002; Gunbin et al., 2011). Cyclin B3 is conserved across metazoans (Lozano et al., 2012). *Ciona intestinalis* cyclin B3 counteracts zygotic transcription (Treen et al., 2018). In *Xenopus laevis*, no cyclin B3 protein was detected in oocytes or the first embryonic divisions (Hochegger et al., 2001), but whether cyclin B3 has a role at these stages has not been addressed. *Drosophila melanogaster* cyclin B3 is dispensable for mitotic divisions and male fertility, but is essential for female fertility (Jacobs et al., 1998). In flies, cyclin B3 promotes anaphase onset in early embryonic divisions (Yuan and O'Farrell, 2015), and loss of cyclin B3 perturbs exit from meiosis I (Jacobs et al., 1998). Moreover, *Drosophila* cyclin B3 is degraded depending on the APC/C in mitosis, with later timing than cyclin A and B (Sigrist et al., 1995; Yuan and O'Farrell, 2015). Unlike in *Drosophila* (Yuan and O'Farrell, 2015), in *Caenorhabditis elegans* embryos cyclin B3 appears to promote anaphase onset in meiosis II and mitosis via the spindle assembly checkpoint (SAC) (van der Voet et al., 2009; Deyter et al., 2010). *C. elegans* and *Drosophila* cyclin B3 associate with CDK1 and support kinase activity *in vitro* (Jacobs et al., 1998; van der Voet et al., 2009).

Cyclin B3 protein is larger in placental mammals due to extension of a single exon (Lozano et al., 2012). Mouse cyclin B3 was proposed to promote recombination in male meiosis because its mRNA is present early in prophase I (Nguyen et al., 2002; Refik-Rogers et al., 2006). Prolonged cyclin B3 expression perturbed spermatogenesis and cyclin B3 interacted with CDK2, although no kinase activity was detected (Nguyen et al., 2002; Refik-Rogers et al., 2006). In females, cyclin B3 was speculated to govern meiotic initiation because its mRNA is upregulated as oogonia cease proliferation and enter prophase I (Miles et al., 2010). RNAi-mediated knock-down of cyclin B3 by ~70% in cultured oocytes perturbed meiosis I progression (Zhang et al., 2015). However, the molecular basis of the progression defect was not defined and RNAi off-target effects could not be excluded, so cyclin B3 function remained unclear.

To sum up, cyclin B3 is implicated in female meiosis and early embryogenesis in different organisms, but its function is poorly understood, particularly in mammals. To gain insights into its potential role(s), we generated mice with a targeted mutation in *Ccnb3*, the gene encoding cyclin B3. Mutant mice are viable, males are fertile, and oocytes enter meiosis. Strikingly, however, most mutant oocytes cannot progress beyond metaphase I, so *Ccnb3*-deficient female mice are sterile. Our data suggest that cyclin B3 fine-tunes APC/C activity towards meiotic substrates in oocyte meiosis I, at least in part as a partner enabling CDK1 catalytic activity, and that the biochemical function of cyclin B3 is conserved in vertebrates.

Results

Female mice are sterile after genetic ablation of *Ccnb3*

Ccnb3 spans 62 kb on the X chromosome and gives rise to a 4.1-kb mRNA of 14 exons encoding a 157.9 kDa protein. CRISPR/Cas9 genome editing generated a 14-bp deletion at the 3′ end of the 2.7-kb long exon 7, causing a frameshift and premature stop codon upstream of the cyclin box in exons 9–13 (**Figure 1A**). Immunoprecipitation/western blotting of extracts from *Ccnb3*$^{-/Y}$ mutant testes yielded no signal for either full-length cyclin B3 or the predicted truncation product (1090 amino acids, ~123 kDa) (**Figure 1B**), indicating that the mutation is a null or severe loss-of-function allele.

Surprisingly, cyclin B3-deficient males were fertile, with no detectable meiotic abnormalities (the male phenotype will be described elsewhere). Heterozygous females had normal fertility and homozygous mutant females were born in Mendelian frequencies (105 +/– (25.7%) : 100 –/– (25.5%) : 102 +/Y (25%) : 101 –/Y (24.8%) offspring from *Ccnb3*$^{+/-}$ females crossed with *Ccnb3*$^{-/Y}$ males). Cyclin B3-deficient animals displayed no gross abnormalities in major organs and tissues (Methods), so cyclin B3 is dispensable in most if not all non-meiotic cells.

Strikingly, however, mutant females were sterile. No pregnancies were observed and no pups were born from *Ccnb3*$^{-/-}$ females (n=9) bred with wild-type males for two rounds of mating. Thus, whereas cyclin B3 is dispensable for male meiosis, it is essential for female fertility.

Cyclin B3 is required for the metaphase-to-anaphase I transition in oocytes

Mammalian female meiosis initiates during fetal development (Herbert et al., 2015; El Yakoubi and Wassmann, 2017). Oocytes complete chromosome pairing and recombination before birth, then enter a prolonged arrest (the dictyate stage) and form primordial follicles, which are the resting pool of germ cells that will be recruited later for ovulation. *Ccnb3*$^{-/-}$ ovary sections showed abundant primordial and growing follicles at 2–3 months of age, and were quantitatively and morphologically indistinguishable from controls (**Figure 1C**). Mutations compromising oogonial development, meiotic initiation, or recombination cause drastically reduced or absent follicles (Di Giacomo et al., 2005; Baltus et al., 2006; Li and Schimenti, 2007; Bolcun-Filas et al., 2014; Jain et al., 2018). The normal number of follicles in *Ccnb3*$^{-/-}$ females therefore implies that cyclin B3 is dispensable for germ cell divisions prior to meiosis and for early events of meiotic prophase I.

We next tested the ability of mutant oocytes to enter meiosis I and to divide. Germinal vesicle (GV) stage oocytes from adult *Ccnb3*$^{-/-}$ mice and age-matched controls from the same breedings (*Ccnb3*$^{+/-}$) were cultured *in vitro*. Germinal vesicle breakdown (GVBD, corresponding to nuclear envelope breakdown in mitosis) occurred with normal timing (within 90 min) and efficiency in *Ccnb3*$^{-/-}$ oocytes **(Figure 1D)**, thus cyclin B3 is dispensable for entry into meiosis I. At ~7–10 hours in culture after GVBD, depending on the mouse strain, oocytes extrude a polar body (PB), indicating execution of the first division and exit from meiosis I (Holt et al., 2013; El Yakoubi and Wassmann, 2017). *Ccnb3*$^{-/-}$ mice had a highly penetrant defect: oocytes from most mutant mice failed to extrude a PB (71 out of 79 mice) (**Figure 1D**). These findings indicate that cyclin B3 is required for progression through meiosis I, and that meiotic progression failure is the cause of female infertility. Because penetrance of meiotic arrest was mouse specific (i.e., most mice yielded only arrested oocytes), we focused on the large majority of mice where no PB extrusion was observed. (For every *Ccnb3*$^{-/-}$ mouse, a fraction of oocytes were matured in the incubator and left untreated to verify that no PB extrusion occurred; see Methods.) Possible reasons for incomplete penetrance are addressed in Discussion.

To further characterize arrest, we followed meiotic progression by live imaging. GV oocytes were injected with mRNA encoding histone H2B fused to RFP and β-tubulin fused to GFP to visualize chromosomes and spindles, respectively. Whereas control oocytes separated their chromosomes and extruded PBs ~8

hours after GVBD, *Ccnb3*$^{-/-}$ oocytes remained in a metaphase I-like state, with a spindle that had migrated to the cortex and chromosomes aligned at the spindle midzone (**Figure 2A, Movies 1 and 2**).

Hypothesizing that mutant oocytes were failing to transition to anaphase I, we predicted that homologous chromosomes would still be conjoined in arrested oocytes. Chromosome spreads from controls had the expected 20 bivalent chromosomes (homolog pairs connected by chiasmata) prior to the first division (6 hours after GVBD) and pairs of sister chromatids juxtaposed near their centromeres afterwards (metaphase II arrest, 16 hours after GVBD) (**Figure 2B**). In contrast, *Ccnb3*$^{-/-}$ oocytes had intact bivalents with no homolog separation throughout the arrest in culture, indicating a metaphase I arrest (**Figure 2B**).

Arrest was not due to failure in forming spindles or stable kinetochore-microtubule interactions, because metaphase I spindles displayed no obvious morphological defects and cold-stable microtubule fibers were comparable to control oocytes in metaphase I (**Figure 2C**). Microtubule fibers attached to kinetochores were clearly visible, so cyclin B3 is not required for kinetochore-microtubule attachments (**Figure 2C**). Spindles in *Ccnb3*$^{-/-}$ oocytes retained the barrel shape characteristic of metaphase I even at late time points 16 hours after GVBD, when control oocytes had progressed to metaphase II, with elongated spindles and more focussed spindle poles (**Figure 2C**).

Arrest in *Ccnb3*$^{-/-}$ oocytes is accompanied by incomplete degradation of APC/C substrates

Separase is a cysteine protease that cleaves the kleisin subunit of cohesin complexes to dissolve sister chromatid cohesion at anaphase onset in mitosis and meiosis (Stemmann et al., 2006). Prior to anaphase, separase activity is restrained in part by binding to its inhibitory chaperone, securin, and by high cyclin B-CDK activity (Stemmann et al., 2006). In oocytes, APC/C-dependent degradation of securin and cyclin B1 activates separase, which cleaves the meiotic kleisin REC8, allowing homologous chromosomes to separate (Herbert et al., 2003; Terret et al., 2003; Kudo et al., 2006). To follow separase activity in live oocytes, we expressed a separase activity sensor (Nikalayevich et al., 2018), similar to one used in cultured mitotic cells (Shindo et al., 2012). The sensor harbors two fluorescent tags separated by a fragment of mitotic kleisin RAD21 as a separase substrate; this ensemble is fused to histone H2B to localize it to chromosomes. Cleavage by separase leaves only the H2B-attached fluorophore on chromosomes (**Figure 3A**). Sensor cleavage occurs only under conditions when endogenous REC8 is removed from chromosome arms (Nikalayevich et al., 2018). In control oocytes, the fluorescent signal on chromosomes changed abruptly from yellow to red upon anaphase onset (**Figure 3B**, top row, compare 6:20 to 6:40). In contrast, both fluorophores remained chromatin-associated throughout arrest in *Ccnbf3*$^{-/-}$

oocytes (**Figure 3B**, bottom row), indicating that separase cannot be activated and explaining why mutant oocytes cannot separate homologous chromosomes and extrude PBs.

Failure to activate separase was potentially due to a failure to degrade cyclin B1 and securin, so we analyzed each protein by western blotting (**Figure 3C**). In control oocytes, levels of both proteins decreased precipitously at anaphase onset (compare 8:30 to 3:30 after GVBD). In *Ccnb3*$^{-/-}$ oocytes in contrast, cyclin B1 levels did not decrease, even at late times. In fact, cyclin B1 levels were consistently higher during arrest (8:30 and later) than in prometaphase (3:30). Securin levels decreased between 3:30 and 8:30 after GVBD, but remained higher than in the controls. Thus, although securin levels drop partially, both proteins are inappropriately stabilized at the time the meiosis I division would normally be carried out.

Next we asked whether cyclin B1 stabilization led to elevated kinase activity in extracts from cultured oocytes. Phosphorylation of histone H1 *in vitro* is mostly attributable to CDK1 plus cyclin B1 (Kubiak et al., 1992; Morgan, 1997; Malumbres et al., 2009) (**Figure 3D**). Control oocytes showed high H1 kinase activity in metaphase I (6:00 after GVBD), and a drop in kinase activity when they extruded PBs (8:00 after GVBD) (Ledan et al., 2001). *Ccnb3*$^{-/-}$ oocytes showed high kinase activity in metaphase I (6:00 after GVBD), but no drop in kinase activity was observed at the time when normal cells extruded PBs (8:00 after GVBD) (**Figure 3D**). These findings suggest that persistence of high cyclin B1 levels in the mutant maintains high CDK1 activity.

Because endogenous securin decreased slightly in *Ccnb3*$^{-/-}$ oocytes (**Figure 3C**), whereas cyclin B1 and H1 kinase activity did not (**Figure 3C, D**), we asked whether inhibiting CDK activity at the normal time of anaphase I onset would suffice for *Ccnb3*$^{-/-}$ oocytes to undergo anaphase I and PB extrusion. Indeed, the CDK inhibitor roscovitine (Meijer et al., 1997) rescued PB extrusion and chromosome segregation, suggesting that meiotic arrest is mainly due to persistently elevated cyclin B1-CDK1 activity (**Figure 3E**).

The results thus far led us to conclude that *Ccnb3*$^{-/-}$ oocytes arrest in metaphase I with aligned bivalents, bipolar spindles, high securin and cyclin B1 protein levels, and little or no separase activity. In oocytes, degradation of cyclin B1 and securin depends on ubiquitination by the APC/C (Herbert et al., 2003; Terret et al., 2003). Hence, our results suggested that without cyclin B3, the APC/C is not sufficiently activated, but because endogenous securin levels did decrease slightly, we suspected that the APC/C might be partially active. To test this, we asked whether exogenously expressed securin and cyclin B1 were also stabilized by live imaging of oocytes injected with mRNAs coding for either protein fused to fluorescent

tags (Herbert et al., 2003; Kudo et al., 2006; Niault et al., 2007; Gui and Homer, 2012; Lane et al., 2012; Rattani et al., 2014). Surprisingly, cyclin B1-GFP and securin-YFP were both efficiently degraded in *Ccnb3*$^{-/-}$ oocytes (**Figure 3F**). Securin-YFP was degraded with kinetics and final extent similar to the controls, whereas cyclin B1-GFP appeared to be degraded slightly more slowly and was higher in *Ccnb3*$^{-/-}$ specifically at the time controls underwent PB extrusion (**Figure 3F**). Thus, even though both exogenous substrates were more efficiently degraded than their endogenous counterparts, the differences between the two substrates were similar in both contexts (i.e., securin was degraded to a greater extent than cyclin B1 in the absence of cyclin B3). These results indicate that the APC/C indeed becomes partially active in the mutants, but further suggest that cyclin B3 specifically promotes degradation of endogenous APC/C substrates. This may be by modulating APC/C specificity *per se*, or by regulating the substrates or their localization to affect their ability to be ubiquitinated.

Timely APC/C activation depends on satisfaction of the SAC (Holt et al., 2013; Touati and Wassmann, 2016), so we asked whether inappropriate SAC activity was the reason for arrest in *Ccnb3*$^{-/-}$ oocytes. Kinetochore recruitment of SAC components, such as MAD2, is a readout for SAC activation (Wassmann et al., 2003; Gui and Homer, 2012; Lischetti and Nilsson, 2015). Similar to controls, MAD2 was recruited to unattached kinetochores early in meiosis I and was not abnormally retained in metaphase I in *Ccnb3*$^{-/-}$ oocytes (**Figure 4A**). We further treated *Ccnb3*$^{-/-}$ oocytes with reversine, which inhibits the SAC kinase MPS1 (Santaguida et al., 2010). Reversine overcame nocodazole-induced arrest in control cells as previously shown (Touati et al., 2015), but did not rescue metaphase arrest caused by cyclin B3 deficiency (**Figure 4B**). We conclude that prolonged SAC activation is not the reason for metaphase I arrest and failure to efficiently degrade endogenous APC/C substrates.

Exogenously expressed cyclin B3 is an APC/C substrate in meiosis

Like other M-phase cyclins, cyclin B3 has a destruction box (D-box) (Nguyen et al., 2002), a motif for APC/C-dependent ubiquitination (Yuan and O'Farrell, 2015) (**Figure 1A**). In mitosis, exogenous cyclin B3 is degraded after cyclin B1 (Nguyen et al., 2002), so we asked about cyclin B3 stability in oocytes. mRNA encoding cyclin B3-RFP was injected into wild-type oocytes together with mRNA for either securin-YFP or cyclin A2-GFP, and oocytes were followed by live imaging. Cyclin B3-RFP accumulated during meiosis I, then was degraded abruptly just before PB extrusion. Importantly, cyclin B3 was degraded after both cyclin A2 and securin (**Figure 5A and B**), showing temporally ordered degradation of APC/C substrates in oocyte meiosis I, at least for exogenous proteins. No re-accumulation of cyclin B3-RFP was observed in meiosis II. Deleting the D-box stabilized cyclin B3-RFP (**Figure 5C**) (there is no

obvious KEN-box or ABBA motif (Davey and Morgan, 2016)). These findings support the conclusion that cyclin B3 is an APC/C substrate in oocytes.

Cyclin B3-associated kinase activity is required for progression through oocyte meiosis I

To test if mouse cyclin B3 supports CDK1 kinase activity as for the *C. elegans*, *Drosophila*, and chicken proteins (Gallant and Nigg, 1994; Jacobs et al., 1998; van der Voet et al., 2009), we expressed and purified from insect cells cyclin B3 N-terminally tagged with maltose binding protein (MBP) and hexahistidine (^{MBPHis}cyclin B3) plus untagged or hemagglutinin (HA) tagged CDK1. Both CDK1 and CDK1-HA co-purified with ^{MBPHis}cyclin B3 on amylose resin (**Figure 6A**, left, lanes 2-3), and both cyclin B3-CDK1 complexes displayed kinase activity towards histone H1 *in vitro* (**Figure 6A**, right, lanes 2-3).

To investigate this kinase activity, we mutated the conserved MRAIL motif on the cyclin fold (Jeffrey et al., 1995; Schulman et al., 1998). MRAIL mutations can prevent binding of cyclin-CDK complexes to substrates without affecting cyclin-CDK interactions (Schulman et al., 1998) or can disrupt cyclin-CDK interaction (Bendris et al., 2011). Mutating the methionine, arginine, and leucine residues of the MRAIL motif to alanine (cyclin B3-MRL mutant) did not affect co-purification of CDK1 (**Figure 6A**, left, lanes 5-6), but eliminated kinase activity (**Figure 6A**, right, lanes 5-6). Furthermore, purification of wild-type cyclin B3 without co-expressed CDK1 yielded detectable kinase activity, presumably attributable to cyclin B3 association with an endogenous insect cell CDK(s), but the MRL mutant gave no such activity (**Figure 6A**, right, lanes 1 and 4). Thus, cyclin B3 can form an active kinase complex with CDK1, suggesting in turn that CDK1 is a physiological partner. We also conclude that the MRL mutant permits CDK1 binding but abolishes associated kinase activity.

We further tested whether oocyte division requires cyclin B3-associated kinase activity. To this end, we first live-imaged *Ccnb3*$^{-/-}$ oocytes injected with mRNA encoding wild-type or D-box deleted (ΔDbox) cyclin B3. Both constructs efficiently rescued PB extrusion (**Figure 6B**). Rescue of MI division by the ΔDbox mutant demonstrated that cyclin B3 degradation is dispensable for anaphase I, and also led us to infer that exogenously expressed cyclin B3 was a quantitatively minor contributor to total CDK1 activity, because high CDK1 should prevent anaphase I. To confirm this idea, we examined H1 kinase activity in synchronized oocytes before and after PB extrusion in rescue experiments. Indeed, *Ccnb3*$^{-/-}$ oocytes rescued by expression of wild-type or ΔDbox cyclin B3 did not show elevated H1 kinase activity in anaphase I (**Figure 6C**, compare lanes 3, 7 and 9). Interestingly though, we found less H1 kinase activity in metaphase I oocytes expressing ΔDbox cyclin B3 (**Figure 6C**, lanes 4, 6 and 8), suggesting that cyclin B1 associated CDK1 kinase activity might be partially downregulated by stable cyclin B3.

Separation of homologous chromosomes was also rescued upon cyclin B3 expression (**Figure 6D**), confirming that meiotic arrest is due to absence of cyclin B3 *per se* and establishing feasibility of structure/function experiments via complementation. In striking contrast to wild-type cyclin B3, the MRL mutant was unable to rescue meiosis I division, PB extrusion, or chromosome segregation (**Figure 6B and D**), indicating that cyclin B3-CDK complexes (likely CDK1) bring about anaphase I onset through their kinase activity towards yet unknown substrates. Note that, unlike cyclin B3, exogenous cyclin B1 did not rescue PB extrusion (**Figure 3F**) or homolog disjunction (**Figure 6D**).

Cyclin B3-CDK1 substrates are likely distinct from cyclin B1-CDK1 substrates, perhaps due to different substrate specificity or accessibility. Furthermore, even though cyclin B3-CDK1 kinase activity is required for PB extrusion, its effect is probably locally restricted and does not lead to a detectable overall increase of CDK1 activity, at least as measured on histone H1 as a substrate.

Functional conservation of vertebrate cyclin B3 in meiosis I

It was previously reported that *X. laevis* oocytes have cyclin B3 mRNA but not detectable protein, from which it was inferred that cyclin B3 plays no role in *Xenopus* oocyte meiosis (Hochegger et al., 2001). Furthermore, cyclin B3 is much larger in mammals than in non-mammalian vertebrates due to the extended exon 7 (Lozano et al., 2012), suggesting the mammalian protein might be functionally distinct. To explore this possibility, we tested for inter-species cross-complementation by injecting mRNAs encoding either *X. laevis* or zebrafish (*Danio rerio*) cyclin B3 into mouse *Ccnb3*$^{-/-}$ oocytes. Remarkably, heterologous expression of cyclin B3 from either species efficiently rescued PB extrusion (**Figure 7A)**. Live imaging showed no obvious defect in chromosome alignment or anaphase I onset in oocytes rescued with *X. laevis* cyclin B3 (**Figure 7B**). The extended exon 7 in mouse cyclin B3 is thus dispensable to promote anaphase I onset. We further infer that cyclin B3 biochemical functions are conserved across vertebrates, in turn raising the possibility that cyclin B3 promotes the oocyte meiosis I division throughout the vertebrate lineage. Even more remarkably, *Drosophila* cyclin B3 was also able to rescue (**Figure 7A**), suggesting conservation of biochemical properties throughout metazoa.

Discussion

Whereas male fertility is unaffected by reduction (Tang et al., 2018), or complete loss (Karasu et al., in preparation) of cyclin B3, mutant females are sterile because cyclin B3 promotes degradation of APC/C substrates and thus triggers anaphase onset in the first meiotic division in oocytes. Similar findings were

obtained with a different *Ccnb3* mutation (Li et al., 2018b *Preprint*). Our findings definitively establish a crucial role for mouse cyclin B3 in the female germline.

The requirement in anaphase I onset is similar to *Drosophila* oocytes (Deyter et al., 2010; Yuan and O'Farrell, 2015). It was proposed that cyclin B3 regulates APC/C activity during the rapid mitotic cycles of the early *Drosophila* embryo (Yuan and O'Farrell, 2015). Our data are consistent with a similar role in mouse oocyte meiosis I. Interestingly, however, exogenous APC/C targets are degraded efficiently in cyclin B3-deficient oocytes but endogenous substrates are not, to our knowledge the first such discrepancy observed. What distinguishes exogenous from endogenous substrates is not clear. One possibility is that expression timing (starting upon mRNA injection into GV oocytes) places exogenous proteins at a disadvantage for binding to essential partners, e.g., of securin to separase and cyclin B1 to CDK. It is also possible that fluorescent protein tags interfere slightly with this binding. Notably, free securin is degraded earlier than separase-bound securin, which is stabilized by maintenance in a non-phosphorylated state through association with phosphatase PP2A (Hellmuth et al., 2014). Securin phosphorylation enhances its affinity for the APC/C (Holt et al., 2008; Hellmuth et al., 2014), and cyclin B3 may control this step. Regardless of the source of the distinction, our data clearly demonstrate that APC/C becomes at least partially active on time, but may not be sufficiently active to robustly provoke degradation of all of its targets.

Alternatively, cyclin B3 may play a repressive role in translation of APC/C substrates after meiosis I entry. After GVBD, cyclin B1 and cyclin B2 mRNA association with polysomes is regulated in a distinct manner in mouse oocytes, resulting in translation of cyclin B1 transcripts but not cyclin B2 (Han et al., 2017). Translational control is crucial because oocytes contain stockpiles of mRNAs required for early embryo development, which are not required during oocyte meiosis (Yang et al., 2017). In principle, the failure of *Ccnb3*$^{-/-}$ mutants to fully downregulate steady-state cyclin B1 and securin levels could mean that cyclin B3-CDK1 represses translation of cyclin B1, securin, and/or other key cell cycle regulators. However, we think this is unlikely, as translation of transcripts coding for cyclin B1 and MOS is induced, not repressed, in a CDK1-dependent manner after GVBD (Han et al., 2017). Nevertheless, we cannot exclude a more indirect role of cyclin B3 in translational control.

We propose that cyclin B3 tips the balance from accumulation of cyclin B1-CDK1 activity towards APC/C-dependent degradation of cyclin B1 and progression into anaphase. Without cyclin B3 the APC/C is active, but endogenous cyclin B1 is not at all, and securin not efficiently, targeted for degradation. Consistent with this view, rescue of *Ccnb3*$^{-/-}$ oocytes by artificially downregulating cyclin B1-CDK1

activity with roscovitine indicates that sufficient separase is liberated from its inhibitory interaction with securin. Cyclin B3 in mammalian oocytes appears dispensable for turning off the SAC, unlike in *C. elegans* (Deyter et al., 2010). Cyclin B3-CDK1 complexes may foster full APC/C activity directly by modifying APC/C substrates, APC/C subunits, APC/C activators (CDC20 and CDH1), or some combination (Alfieri et al., 2017). The robustness of the arrest is comparable to that observed when maintaining high cyclin B1 levels (e.g., with non-degradable cyclin B1 (Herbert et al., 2003; Touati et al., 2012)), but not SAC activation, which is transient (Touati and Wassmann, 2016).

Nevertheless, cyclin B3 is not strictly essential, in that some mice (~10% of those assayed thus far) harbored oocytes able to progress through meiosis I. This incomplete penetrance may reflect subtle variation (perhaps from strain background) in either the degree of APC/C activation or the threshold of APC/C activity needed for progression. Put another way, cyclin B3-deficient oocytes may occasionally achieve just enough APC/C activity during a critical time window to cross a threshold needed for the switch-like transition into anaphase I.

In budding and fission yeast, sequential substrate phosphorylation during cell cycle progression is thought to be primarily via changes in overall CDK activity as opposed to substrate specificities of different cyclins (Stern and Nurse, 1996; Coudreuse and Nurse, 2010; Bouchoux and Uhlmann, 2011; Uhlmann et al., 2011). Accordingly, the cell cycle can be driven by a single CDK-cyclin fusion complex in *S. pombe* (Coudreuse and Nurse, 2010; Swaffer et al., 2016). In mouse, CDK1 is the only CDK essential for mitotic cell cycle progression *per se* (Santamaria et al., 2007). Loss of cyclin B2 does not affect viability or fertility, indicating that cyclin B1 is sufficient (Brandeis et al., 1998). It may thus seem surprising that cyclin B3 has such a specific role in oocyte meiosis that cannot be replaced by cyclin B1. Hence, cell cycle progression in meiosis appears to be specifically dependent on individual CDK complexes. This conclusion is further supported by the fact that loss of CDK2 does not affect somatic cells but leads to sterility due to failure to enter meiosis I (Ortega et al., 2003). Cell type specificity is also seen for cyclin A2, which is required in hematopoetic stem cells, fibroblasts, and female meiosis, but not in other tissues (Kalaszczynska et al., 2009; Touati et al., 2012; Zhang et al., 2017).

Overall, our data show that cyclin B3 is an M-phase cyclin with a singular role in oocyte meiosis, probably due to the specificities of meiotic cell cycle regulation in this huge cell. A key challenge now will be to determine whether APC/C activity or substrate accessibility is directly dependent on cyclin B3-CDK activity, and to define relevant phosphorylation targets needed for proper meiotic progression.

Materials and methods

Further information and requests for resources and reagents should be directed to and will be fulfilled by the corresponding authors, Scott Keeney (s-keeney@ski.mskcc.org) and Katja Wassmann (katja.wassmann@upmc.fr).

Animals

Mice in the SK lab were maintained under regulatory standards approved by the Memorial Sloan Kettering Cancer Center (MSKCC) Institutional Animal Care and Use Committee. Mice in the KW lab were maintained according to current French guidelines in a conventional mouse facility (UMR7622), with authorization C 75-05-13. All experiments were subject to ethical review and approved by the French Ministry of Higher Education and Research (authorization n° B-75-1308). For this study females were either purchased at 7 weeks of age (CD-1 mice, Janvier Lab France), and used at 8-16 weeks of age for experiments, or bred in our animal facilities and used at 8-16 weeks of age (*Ccnb3* mouse strain). Except for genotyping, the mice had not been involved in any procedures prior to experimentation and they were given *ad libitum* access to food and water supply. Housing was done under a 12 hour light / 12 hour dark cycle according to the Federation of European Laboratory Science Associations (FELASA).

Generation of *Ccnb3* knock-out mouse strain, husbandry and genotyping

Endonuclease mediated (*em*) allele was generated by the MSKCC Mouse Genetics Core Facility. Exon 7 of *Ccnb3* (NCBI Gene ID: 209091) was targeted by guide RNA (C40-TGAACTTGGCATGATAGCAC). (Exon numbering used here is from the current accession. The targeted exon corresponds to exon 8 in the numbering used by Lozano et al. (Lozano et al., 2012).) Guide RNA was cloned into pDR274 vector for *in vitro* transcription. *In vitro* transcribed guide RNA (10 ng/μl) and Cas9 (20 ng/μl) were microinjected into pronuclei of CBA/J × C57BL/6J F2 hybrid zygotes using conventional techniques (Romanienko et al., 2016).

Genomic DNA from founder animals were subjected to PCR by using following primers, CCN3B-A GAGTATTAGCACTGAGTCAGGGAC and CCN3B-B GGAATACCTCAGTTTCTTTTGCAC and T7 endonuclease I digestion was performed to identify the animals carrying indels. Since male animals have one copy of the X-linked *Ccnb3* gene, T7 assay on males was performed in the presence of wild-type genomic DNA.

To define the molecular nature of indels, genomic DNA from T7-positive animals was amplified using the primers indicated above. Amplified PCR fragments were used for TA Cloning (TA Clonining™ Kit with pCR™ 2.1 vector, Invitrogen). Ten white bacterial colonies were selected, inserts were sequenced, and the mutations were characterized as deletions, insertions or substitutions. The *em1* allele, an out-of-frame deletion, was chosen to generate the *Ccnb3*^{em1Sky} line. After two rounds of backcrossing to C57BL/6J, animals were interbred to generate homozygous and heterozygous female animals and hemizygous male animals. Primers for genotyping were GT4-F TGTTGATGAAGAGGAATTTTTCAAATCATTCCT and GT4-R TTCTTTTGCACCCAGAGTTGACTTAAAG. The amplified PCR product was subjected to BsrI enzyme digestion (NEB). A BsrI site is lost in the *em1* allele. Since *Ccnb3* is X-linked, no *Ccnb3*$^{+/+}$ females can be obtained through crosses yielding homozygous *Ccnb3*$^{-/-}$ mice. Therefore, we bred *Ccnb3*$^{-/Y}$ males with *Ccnb3*$^{+/-}$ females to obtain *Ccnb3*$^{-/-}$ and *Ccnb3*$^{+/-}$ females to use as experimental mice and littermate controls, respectively.

Oocyte harvesting and *in vitro* culture

GV-stage oocytes were collected from ovaries of sacrificed CD-1 mice or *Ccnb3*$^{+/-}$ and *Ccnb3*$^{-/-}$ mice aged 8-16 weeks. Ovaries were transferred to drops of homemade M2 medium at 38°C and dissected to obtain oocytes. Oocytes were collected and isolated from follicular cells with mouth pipetting using torn-out Pasteur pipettes. For all microinjection experiments, ovaries and oocytes were incubated in drops of commercial M2 medium (Sigma-Aldrich) and kept at GV stage by the addition of dibutyl cyclic AMP (dbcAMP, Sigma-Aldrich) at 100 µg/ml final concentration. Oocytes undergoing GVBD within at most 90 min after ovary dissection or release from dbcAMP were used for experiments. For all experiments using *Ccnb3*$^{-/-}$ mice, for every *Ccnb3*$^{-/-}$ mouse at least 5 mature GVBD-stage oocytes were left untreated and released in parallel to control oocytes to ascertain that no PB extrusion occurred. In the rare cases where PB extrusion occurred in *Ccnb3*$^{-/-}$ oocytes, the experiment (this was especially important for the rescue experiments in Figures 3E, 4B, 6B-D, and 7A,B) was aborted and not taken into account. Where indicated, roscovitine was added 6:20 after GVDB at a final concentration of 0.2 mM, nocodazole was added at 6:00 after GVBD at a final concentration of 400 nM, and reversine at 6:40 after GVBD at a final concentration of 500 nM. Because it is soluble in oil, reversine was also added to the oil covering the media drops.

Histology

Ovaries from *Ccnb3*$^{+/-}$ and *Ccnb3*$^{-/-}$ adult mice were fixed overnight in 4% paraformaldehyde (PFA) at 4°C. Fixed tissues were washed in water and stored in 70% ethanol at 4°C. Fixed tissues were submitted to the Molecular Cytology Core Facility (MSKCC) for embedding in paraffin and sectioning of the embedded tissue (whole ovary) as 8 µm sections and preparation of slides with ovary sections. The slides

were then subjected to immunohistochemistry as follows: The immunohistochemical staining was performed at Molecular Cytology Core Facility (MSKCC) using a Discovery XT processor (Ventana Medical Systems). Ovary sections were de-paraffinized with EZPrep buffer (Ventana Medical Systems), antigen retrieval was performed with CC1 buffer (Ventana Medical Systems). Sections were blocked for 30 minutes with Background Buster solution (Innovex), followed by avidin-biotin blocking for 8 minutes (Ventana Medical Systems). Sections were then incubated with anti-VASA (Abcam, cat#ab13840, 0.17 µg/ml) for 5 hours, followed by 60 minutes incubation with biotinylated goat anti- rabbit (Vector Labs, cat# PK6101) at 1:200 dilution. The detection was performed with DAB detection kit (Ventana Medical Systems) according to manufacturer instruction. Slides were counterstained with hematoxylin and cover slipped with Permount (Fisher Scientific). IHC slides were scanned using Pannoramic Flash 250 with a 20×/0.8 NA air objective. Images were analyzed using Pannoramic Viewer Software (3DHistech). To count oocytes, every fifth section on the slide was analyzed and the number of oocytes in primordial, primary, secondary and antral follicles were noted and summed.

Histological examination of somatic tissues

Gross histopathological analysis of major organs and tissues was performed by the MSKCC Laboratory of Comparative Pathology Core Facility for the following mice: two 2-month old *Ccnb3*$^{-/Y}$ males and one 2-month old *Ccnb3*$^{+/Y}$ male; two 5-month old *Ccnb3*$^{-/-}$ females and two 5-month old *Ccnb3*$^{+/-}$ females. Histological examination of following tissues was performed: diaphragm, skeletal muscle, sciatic nerve, heart/aorta, thymus, lung, kidneys, salivary gland, mesenteric lymph nodes, stomach, duodenum, pancreas, jejunum, ileum, cecum, colon, adrenals, liver, gallbladder, spleen, uterus, ovaries, cervix, urinary bladder, skin of dorsum and subjacent brown fat, skin of ventrum and adjacent mammary gland, thyroid, parathyroid, esophagus, trachea, stifle, sternum, coronal sections of head/brain, vertebrae and spinal cord. Tissues were fixed in 10% neutral buffered formalin and bones were decalcified in formic acid solution using the Surgipath Decalcifier I (Leica Biosystems) for 48 hr. Samples were routinely processed in alcohol and xylene, embedded in paraffin, sectioned (5 µm), and stained with hematoxylin and eosin. Examined tissues and organs were grossly normal.

Extract preparation and western blotting

To analyze endogenous protein levels, oocytes were cultured as described above. Oocytes were harvested at the indicated time points, washed in phosphate buffer saline (PBS) to remove proteins from the medium and then placed on the wall of the Eppendorf tube and snap-frozen in liquid nitrogen. Later, 7.5 µl 1× Laemmli lysis buffer was added to the tube and samples were boiled 5 minutes at 100°C.

For western blotting, samples were separated on 4–12% Bis-Tris NuPAGE precast gels (Life Technologies) at 150 V for 70 minutes. Proteins were transferred to polyvinylidene difluoride (PVDF) membranes by wet transfer method in Tris-Glycine-20% methanol, at 120 V for 40 minutes at 4°C. Membranes were blocked with 5% non-fat milk in PBS-0.1% Tween (PBS-T) for 30 minutes at room temperature on an orbital shaker. Blocked membranes were incubated with primary antibodies 1 hr at room temperature or overnight at 4°C. Membranes were washed with PBS-T for 30 minutes at room temperature, then incubated with HRP-conjugated secondary antibodies for 1 hr at room temperature. Membranes were washed with PBS-T for 15 minutes and the signal was developed by ECL Plus Perkin Elmer or ECL Prime GE Healthcare.

To analyse cyclin B3 protein levels from mouse testis extracts, dissected testes were placed in an Eppendorf tube, frozen on dry ice and stored at -80°C. The frozen tissue was resuspended in RIPA buffer (50 mM Tris-HCL pH 7.5, 150 mM NaCl, 0.1% SDS, 0.5% sodium deoxycholate, 1% NP40) supplemented with protease inhibitors (Roche, Mini tablets). The tissue was disrupted with a plastic pestle and incubated by end-over-end rotation for 15 minutes, at 4°C. After brief sonication, samples were centrifuged at 15000 rpm for 15 minutes. The cleared lysate was transferred to a new tube, and used for immunoprecipitation. Whole cell extract was pre-cleared with protein G beads by end-over-end rotation for 1 hr, at 4°C. Anti-cyclin B3 monoclonal antibody (10 µg; Abmart Inc., clone number 19584-1R1-3/C500_140905, raised against the epitope SNMEKEFILDIPNK (amino acids 110–123)) was then added to the pre-cleared lysates and incubated overnight with end-over-end rotation, at 4°C. Protein G beads were added to the tubes and incubate for 1 hr with end-over-end rotation, at 4°C. Beads were washed three times with RIPA buffer, resuspended in 1x NuPAGE LDS sample buffer (Invitrogen) with 50 mM DTT, and boiled 5 minutes to elute immunoprecipitated proteins.

Primary antibodies were used at the following dilutions to detect proteins: mouse anti-securin (ab3305, Abcam, 1:300), mouse anti-cyclin B1 (ab72, Abcam, 1:400), mouse anti-β actin (8H10D10, CST,1:1000), mouse anti-cyclin B3 (Abmart Inc, 1:500), and rat anti-tubulin alpha (MCA78G, Biorad, 1:1000). Secondary antibodies were used at the following dilutions: goat anti-mouse IgG (H+L)-HRP (1721011, Biorad, 1:10000), and goat anti-rat IgG-HRP (AP136P, Millipore, 1:10000).

Plasmids

Mouse *Ccnb3* mRNA was amplified by PCR from whole testis cDNA library and cloned into pRN3-RFP vectors using the In-Fusion cloning kit (Clontech, Takara). *X. laevis cyclin B3* cDNA (clone ID: 781186, NCBI ID: 379048) was purchase from Dharmacon and used as a template for PCR amplification. *D. rerio*

and *D. melanogaster cyclin B3* (NCBI ID: 767751 and 42971, respectively) were amplified by PCR from cDNA from *D. rerio* embryo or the S2 cell line, respectively. Amplified products for *X. laevis*, *D. rerio* and *D. melanogaster* were cloned into pRN3-GFP vector using the In-Fusion cloning kit (Clontech, Takara). To generate *Ccnb3* MRL mutation, overlapping primers with specific mutation were used to amplify PCR product from the wild-type template pRN3-cyclin B3-RFP, the template was digested by DpnI treatment, and the PCR product was used to transform *E. coli* DH5α competent cells. To generate the ΔD-box mutation, PCR primers that delete the D-box were used to amplify the *Ccnb3* plasmid, and the resulting PCR product was phosphorylated and ligated. Primer list can be found as **Table S1**. Plasmids for in vitro transcription of cyclin B1-GFP, securin-YFP, histone H2B-RFP, cyclin A2-GFP and β-tubulin-GFP have been used (Brunet et al., 1998; Herbert et al., 2003; Terret et al., 2003; Tsurumi et al., 2004; Touati et al., 2012)

Expression and purification of recombinant proteins

Vectors for expression of cyclin B3 (wild type or MRL mutant) N-terminally tagged with maltose-binding protein and 6x histidine were generated by cloning in pFastBac1-MBP6XHis. Wild-type *Ccnb3* was amplified from pRN3-cyclin B3-RFP and the MRL mutant was amplified from pRN3-*cyclin B3 MRL*-RFP. The plasmid was digested with SspI restriction endonucleases. By using In-Fusion cloning kit (Clontech, Takara) the PCR products were cloned into SspI linerazed plasmid. Viruses were produced by a Bac-to-Bac Baculovirus Expression System (Invitrogen) following the manufacturer's instructions. Baculovirus expressing CDK1 and CDK1-HA were generously supplied by Dr. R. Fisher (Desai et al., 1992).

To express ^{MBPHis}cyclin B3 and ^{MBPHis}cyclin B3 MRL alone, *Spodoptera frugiperda* Sf9 cells were infected with virus at a multiplicity of infection (MOI) of 3. To express ^{MBPHis}cyclin B3-CDK1or CDK1-HA and ^{MBPHis}cyclin B3 MRL-CDK1or CDK1-HA complexes, Sf9 cells were infected with both viruses at a multiplicity of infection (MOI) of 3 and 2, respectively. Cells from two 150 mm plastic dishes per infection (each containing ~ 3×10^7 cells) were harvested 48 hours after infection by centrifugation at 1500 rpm for 5 minutes and then washed with ice-cold PBS. Cell pellets were resuspended in 1.7 ml of ice-cold lysis buffer (25 mM HEPES-NaOH pH 7.5, 150 mM NaCl, 100 μM leupeptin (Sigma-Aldrich, L2884)), 1× Complete protease inhibitor tablet (Roche) and 0.5 mM phenylmethanesulfonyl fluoride (PMSF)). Cells were lysed by sonication and centrifuged at 15000 rpm for 30 minutes, at 4°C. The cleared extract was moved to a 2 ml Eppendorf tube and mixed with 300 μl slurry of amylose resin (NEB, E802L) pre-equilibrated with lysis buffer. After 1 hour at 4°C with end-over-end rotation, the amylose resin was centrifuged at 300 *g*, for 1 minute, at 4°C. Resin was washed briefly with ice-cold lysis buffer before

transfer on Bio-Spin chromatography columns (BioRad, 7326008). The resin on the column was washed five times with ice-cold wash buffer (lysis buffer plus 10% glycerol). To elute the proteins from the column, the resin was incubated with 100–200 μl ice-cold elution buffer (wash buffer plus 10 mM maltose (Sigma, M5885)). All steps during the purification were done at 4°C.

Histone H1 kinase assay with recombinant proteins expressed in Sf9 cells

Eluates from the amylose affinity purification step were used for histone H1 kinase assays. Reactions were performed in 10 mM HEPES-NaOH pH 7.4, 75 mM NaCl, 1 mM DTT, 10 mM $MgCl_2$, 100 μM ATP (Roche, 11140965001), 1 μCi [γ-^{32}P] ATP and histone H1 (5 μg/μl) (Sigma, 10223549001). 10 μl reaction mix was added to 10 μl eluate from the amylose resin and incubated for 30 minutes at room temperature. To terminate reactions, 5 μl of 4× SDS sample buffer was added to each reaction and samples were boiled for 5 mins before loading on 12% NuPage Bis-Tris NuPAGE precast gels (Life Technologies). Samples were subjected to electrophoresis at 150 V for 60 minutes. The gel was then vacuum dried for 45 minutes, at 80°C. Radiolabelled species were imaged using a Fuji phosphoimager and analyzed by Image Gauge software.

Histone H1 kinase assays using oocyte extracts

Kinase assays to determine endogenous kinase activity were performed on aliquots of 5 oocytes at the indicated stages of meiotic maturation (Kudo et al., 2006). In short, oocytes were lysed in 3 μl of lysis buffer ((50 mM Tris (pH 7.5), 150 mM NaCl, 1% Igepal (Sigma), 10% glycerol, 2 mM EDTA, supplemented with protease inhibitors (Roche, Mini tablets) on ice for 20 minutes before adding 6 μl kinase assay buffer (50mM Tris (pH 7.5), 150 mM NaCl, 10mM $MgCl_2$, 0.5 mM DTT, 2.5 mM EGTA, 150 μM ATP) supplemented with 3 μCi of [γ-^{32}P]ATP (Perkin Elmer) per sample. Histone H1 (Millipore, 0.5 μg per sample) was used as a substrate. Kinase reactions were incubated 30 min at 30°C, denatured, and analyzed by SDS-PAGE. The gel was fixed and dried before being exposed and scanned to detect incorporation of [γ-^{32}P]ATP into the substrate, using a Typhoon FLA9000 phosphorimager (GE Healthcare Life Sciences). Scans were analyzed by ImageJ.

Microinjection and live imaging

In vitro transcription of all mRNAs was done using the Ambion mMessage Machine kit according to the manufacturer's instructions. mRNAs (1 to 10 pM) were purified on RNeasy purification columns (Qiagen). GV stage oocytes were microinjected with mRNA on an inverted Nikon Eclipse Ti microscope. Microinjection pipettes were made using a magnetic puller (Narishige PN-30). Oocytes were manipulated with a holding pipette (VacuTip from Eppendorf) and injection was done using a FemtoJet Microinjector

pump (Eppendorf) with continuous flow. Injection of the oocytes was done on a Tokai Hit temperature controlled glass plate at 38°C. Live imaging of oocytes in Figures 3B, 3E and 7B, and supplemental movies 1 and 2 was carried out on an inverted Zeiss Axiovert 200M microscope coupled to an EMCCD camera (Evolve 512, Photometrics), combined with an MS-2000 automated stage (Applied Scientific Instrumentation), a Yokogawa CSU-X1 spinning disc and a nanopositioner MCL Nano-Drive and using a Plan-APO (40×/1.4 NA) oil objective (Zeiss). Images of chromosomes were acquired with 11 z-sections of 3 µm, except otherwise mentioned. For live imaging Figures 2A, 3F, 5A-C, and 6B, a Nikon eclipse TE 2000-E inverted microscope with motorized stage, equipped with PrecisExite High Power LED Fluorescence (LAM 1: 400/465, LAM 2: 585), a Märzhäuser Scanning Stage, a CoolSNAP HQ2 camera, and a Plan APO (20×/0.75 NA) objective was used. One section in z was acquired for all movies except movies for Figure 2A where 11 z-sections of 3 µm were acquired. Both microscopes were controlled by Metamorph software and all live imaging was done in commercial M2 medium (Sigma-Aldrich) covered by mineral oil (embryo certified, Sigma) at 38°C. All images were stacked and assembled using ImageJ. Quantifications were done on untreated images. For Figures, brightness was adjusted with the same parameters per experimental condition with ImageJ.

Chromosome spreads and immunofluorescence

Oocytes were rinsed in successive drops of Tyrode's acid solution to remove their *zona pellucida.* For chromosome spreads, oocytes were fixed at room temperature using a spread solution (1% paraformaldehyde, 0.15% Triton X-100 and 3 mM DTT, from Sigma-Aldrich), at the time points indicated. For whole-mount immunofluorescence, chambers were coated with concanavaline A (Sigma-Aldrich) in M2 PVP (polyvinylpyrrolidone 0,1mM from Merck-Millipore) medium and oocytes were placed in the chambers and centrifuged at 1400 rpm for 13 min at 38°C. Oocytes were then placed in a cold treatment solution (20 mM HEPES-NaOH, 1 mM $MgCl_2$, pH 7.4) on top of ice (4°C) for 4 min to remove unstable microtubules. Following cold treatment, oocytes were incubated in a formaldehyde fixation solution (BRB80 medium with 0.3% Triton X-100, 1.9% formaldehyde (Sigma-Aldrich)) at 38°C for 30 min. Primary antibodies were used at the indicated concentrations: human CREST serum autoimmune antibody against centromere (Immunovision, HCT-0100, 1:100), rabbit polyclonal anti-MAD2 (1:50)(Wassmann and Benezra, 1998), and mouse monoclonal anti-alpha-tubulin (DM1A) coupled to FITC (Sigma-Aldrich, F2168, 1:100). Secondary antibodies were used at the following concentrations: anti-human Alexa 488 (Life Technologies, A11013, 1:200), anti-human Cy3 (Jackson ImmunoResearch, #709-166-149, 1:200), anti-rabbit Cy3 (Jackson ImmunoResearch, #711-166-152, 1:200). Hoechst 3342 (Invitrogen, H21492) at 50 µg/ml was used to stain chromosomes and AF1 Cityfluor mounting medium was used.

Image acquisitions of fixed oocytes

An inverted Zeiss Axiovert 200M microscope as described above for live imaging was used to image chromosome spreads and for whole mount immunofluorescence acquisitions, using a 100×/1.4 NA oil objective coupled to an EMCCD camera (Evolve 512, Photometrics). Six z-sections of 0.4 μm were taken for spreads, and 11 z-sections of 1 μm for whole mount oocytes. Stacks acquired with Metamorph software were assembled in ImageJ. Quantifications were done on untreated acquisitions. For Figures, brightness was adjusted with the same parameters per experimental condition, using ImageJ.

Quantification of fluorescent signals

For the quantification of MAD2 fluorescence signal, the intensity was calculated for each kinetochore using an 8 × 8 pixels square on the kinetochore (where CREST signal is located). The same sized square was used adjacent to the MAD2 fluorescence to measure background, which was subtracted from the MAD2 signal. The MAD2 fluorescence intensity was normalized to the CREST signal of the same kinetochore. For the cyclin B3-RFP, ΔDbox cyclin B3-RFP, cyclin A2-GFP, cyclin B1-GFP, and securin-YFP quantifications, a 150 × 150 pixels circle was placed in the center of each oocyte for the fluorescence intensity signal measurement, and another placed adjacent to the oocyte to measure background. For each oocyte, background-subtracted values were normalized relative to the highest value. All measurements were done using ImageJ software on untreated acquisitions.

Statistical analysis

For statistical analysis, GraphPad Prism 7 was used. For the comparison of independent samples, unpaired Student's t test was carried out. Error bars indicate means +/- standard deviation. Sample size and statistical tests are indicated in the figure and figure legends, respectively. Selection of oocytes for different conditions was at random. No statistical analysis was used to determine sample size. Collection and analysis of the data were not performed blind to the conditions of the experiments, no data from experiments were excluded from analysis. The number of independent replicates is indicated in the figure legends.

Supplementary material:

Two movies showing chromosome movements in a representative control (Movie 1) and a *Ccnb3*$^{-/-}$ oocyte (Movie 2).

One table providing sequence information for the primers used in this study.

Abbreviations used:

APC/C, anaphase-promoting complex/cyclosome; GV, germinal vesicle; GVBD, germinal vesicle breakdown; PB, polar body; SAC, spindle assembly checkpoint

Acknowledgements

We thank W. Li, Q. Zhou, and Y. Zhang (State Key Laboratory of Stem Cell and Reproductive Biology) for sharing unpublished data; A. Koff (MSKCC) for sharing unpublished data, discussions, and critical reading of the manuscript; P. Romanienko, W. Mark, J. Ingenito and J. Giacalone (MSKCC Mouse Genetics Core Facility) for generating mutant mice and J. White (MSKCC Laboratory of Comparative Pathology Core Facility) for anatomic pathology; R. Fisher (Icahn School of Medicine at Mount Sinai) for CDK1 and CDK1-HA baculoviruses and advice for CDK expression and H1 kinase assays with purified proteins; C. Claeys Bouuaert (Keeney lab) for help with baculovirus expression and protein purification; M. Boekhout and D. Ontoso (Keeney lab) for help with animal handling; B. Joseph (MSKCC) for *Drosophila* cDNA, M. Jelcic and C. Huang (MSKCC) for *D. rerio* cDNA, and H. Funabiki (Rockefeller University) for *Xenopus* cDNA; N. Fang, M. Turkekul, A. Barlas and K. Manova-Todorova (MSKCC Molecular Cytology Core Facility) for help with ovarian histology; members of the Wassmann and Keeney labs for discussion; S. Touati (Crick, London) and A. Karaiskou (CDR Saint Antoine, Paris) for comments on the manuscript; A. Dupré (IBPS) for discussion, E. Nikalayevich (Wassmann lab) for help with the separase sensor assay; F. Passarelli (Wassmann lab) for help with rescue experiments in Figure 7; C. Rachez (Institut Pasteur, Paris) for access to the phosphorimager; and D. Cladière (Wassmann lab) for technical help and animal handling. MSKCC core facilities were supported by NIH grant P30 CA008748. NB received a 3-year PhD fellowship from the French Ministère de la Recherche, and a 1-year fellowship by the Fondation ARC pour la Recherche sur le Cancer. Work in the Wassmann lab was financed through a grant "Equipe FRM" by the Fondation de la Recherche Médicale (Equipe DEQ20160334921 to KW), an ANR grant (ANR-16-CE92-0007-01 to KW), and core funding from UPMC and the CNRS. Work in the Keeney lab was supported by the Howard Hughes Medical Institute. The authors declare no competing financial interests.

Author Contributions

Mehmet Karasu generated the *Ccnb3*$^{-/-}$ mouse strain and cloned plasmids used in this study, unless otherwise noted, and performed experiments in Figures 1A-C, 3C, and 6A. Experiments in Figures 4A, and B, 6B and C, and 7A and B were performed by Nora Bouftas, and kinase assays in Figure 3D and 6C by Nora Bouftas and Katja Wassmann The remaining experiments and statistical analysis were done by Nora Bouftas and Mehmet Karasu. Overall supervision, funding acquisition and project administration

were done by Katja Wassmann and Scott Keeney. Figures were prepared by Nora Bouftas, Mehmet Karasu, and Katja Wassmann, and the manuscript was written by Katja Wassmann and Scott Keeney with substantial input from other authors.

References

Alfieri, C., S. Zhang, and D. Barford. 2017. Visualizing the complex functions and mechanisms of the anaphase promoting complex/cyclosome (APC/C). *Open Biol*. 7. pii: 170204.

Baltus, A.E., D.B. Menke, Y.C. Hu, M.L. Goodheart, A.E. Carpenter, D.G. de Rooij, and D.C. Page. 2006. In germ cells of mouse embryonic ovaries, the decision to enter meiosis precedes premeiotic DNA replication. *Nat Genet*. 38:1430-1434.

Bendris, N., B. Lemmers, J.M. Blanchard, and N. Arsic. 2011. Cyclin A2 mutagenesis analysis: a new insight into CDK activation and cellular localization requirements. *PLoS One*. 6:e22879.

Bolcun-Filas, E., V.D. Rinaldi, M.E. White, and J.C. Schimenti. 2014. Reversal of female infertility by Chk2 ablation reveals the oocyte DNA damage checkpoint pathway. *Science*. 343:533-536.

Bouchoux, C., and F. Uhlmann. 2011. A quantitative model for ordered Cdk substrate dephosphorylation during mitotic exit. *Cell*. 147:803-814.

Brandeis, M., I. Rosewell, M. Carrington, T. Crompton, M.A. Jacobs, J. Kirk, J. Gannon, and T. Hunt. 1998. Cyclin B2-null mice develop normally and are fertile whereas cyclin B1-null mice die in utero. *Proc Natl Acad Sci U S A*. 95:4344-4349.

Brunet, S., Z. Polanski, M.H. Verlhac, J.Z. Kubiak, and B. Maro. 1998. Bipolar meiotic spindle formation without chromatin. *Curr Biol*. 8:1231-1234.

Coudreuse, D., and P. Nurse. 2010. Driving the cell cycle with a minimal CDK control network. *Nature*. 468:1074-1079.

Davey, N.E., and D.O. Morgan. 2016. Building a Regulatory Network with Short Linear Sequence Motifs: Lessons from the Degrons of the Anaphase-Promoting Complex. *Mol Cell*. 64:12-23.

Desai, D., Y. Gu, and D.O. Morgan. 1992. Activation of human cyclin-dependent kinases in vitro. *Mol Biol Cell*. 3:571-582.

Deyter, G.M., T. Furuta, Y. Kurasawa, and J.M. Schumacher. 2010. Caenorhabditis elegans cyclin B3 is required for multiple mitotic processes including alleviation of a spindle checkpoint-dependent block in anaphase chromosome segregation. *PLoS Genet*. 6:e1001218.

Di Giacomo, M., M. Barchi, F. Baudat, W. Edelmann, S. Keeney, and M. Jasin. 2005. Distinct DNA-damage-dependent and -independent responses drive the loss of oocytes in recombination-defective mouse mutants. *Proc Natl Acad Sci U S A*. 102:737-742.

El Yakoubi, W., and K. Wassmann. 2017. Meiotic Divisions: No Place for Gender Equality. *Adv Exp Med Biol*. 1002:1-17.

Fisher, D., L. Krasinska, D. Coudreuse, and B. Novak. 2012. Phosphorylation network dynamics in the control of cell cycle transitions. *J Cell Sci*. 125:4703-4711.

Gallant, P., and E.A. Nigg. 1994. Identification of a novel vertebrate cyclin: cyclin B3 shares properties with both A- and B-type cyclins. *EMBO J*. 13:595-605.

Gui, L., and H. Homer. 2012. Spindle assembly checkpoint signalling is uncoupled from chromosomal position in mouse oocytes. *Development*. 139:1941-1946.

Gunbin, K.V., V.V. Suslov, Turnaev, II, D.A. Afonnikov, and N.A. Kolchanov. 2011. Molecular evolution of cyclin proteins in animals and fungi. *BMC Evol Biol*. 11:224.

Han, S.J., J.P.S. Martins, Y. Yang, M.K. Kang, E.M. Daldello, and M. Conti. 2017. The Translation of Cyclin B1 and B2 is Differentially Regulated during Mouse Oocyte Reentry into the Meiotic Cell Cycle. *Sci Rep*. 7:14077.

Heim, A., B. Rymarczyk, and T.U. Mayer. 2017. Regulation of Cell Division. *Adv Exp Med Biol*. 953:83-116.

Hellmuth, S., F. Bottger, C. Pan, M. Mann, and O. Stemmann. 2014. PP2A delays APC/C-dependent degradation of separase-associated but not free securin. *EMBO J*. 33:1134-1147.

Herbert, M., D. Kalleas, D. Cooney, M. Lamb, and L. Lister. 2015. Meiosis and Maternal Aging: Insights from Aneuploid Oocytes and Trisomy Births. *Cold Spring Harb Perspect Biol*. 7.

Herbert, M., M. Levasseur, H. Homer, K. Yallop, A. Murdoch, and A. McDougall. 2003. Homologue disjunction in mouse oocytes requires proteolysis of securin and cyclin B1. *Nat Cell Biol*. 5:1023-1025.

Hochegger, H., A. Klotzbucher, J. Kirk, M. Howell, K. le Guellec, K. Fletcher, T. Duncan, M. Sohail, and T. Hunt. 2001. New B-type cyclin synthesis is required between meiosis I and II during Xenopus oocyte maturation. *Development*. 128:3795-3807.

Holt, J.E., S.I. Lane, and K.T. Jones. 2013. The control of meiotic maturation in mammalian oocytes. *Current topics in developmental biology*. 102:207-226.

Holt, L.J., A.N. Krutchinsky, and D.O. Morgan. 2008. Positive feedback sharpens the anaphase switch. *Nature*. 454:353-357.

Jacobs, H.W., J.A. Knoblich, and C.F. Lehner. 1998. Drosophila Cyclin B3 is required for female fertility and is dispensable for mitosis like Cyclin B. *Genes Dev*. 12:3741-3751.

Jain, D., M.R. Puno, C. Meydan, N. Lailler, C.E. Mason, C.D. Lima, K.V. Anderson, and S. Keeney. 2018. *ketu* mutant mice uncover an essential meiotic function for the ancient RNA helicase YTHDC2. *Elife*. 7. pii: e30919

Jeffrey, P.D., A.A. Russo, K. Polyak, E. Gibbs, J. Hurwitz, J. Massague, and N.P. Pavletich. 1995. Mechanism of CDK activation revealed by the structure of a cyclinA-CDK2 complex. *Nature*. 376:313-320.

Kalaszczynska, I., Y. Geng, T. Iino, S. Mizuno, Y. Choi, I. Kondratiuk, D.P. Silver, D.J. Wolgemuth, K. Akashi, and P. Sicinski. 2009. Cyclin A is redundant in fibroblasts but essential in hematopoietic and embryonic stem cells. *Cell*. 138:352-365.

Kubiak, J.Z., M. Weber, G. Geraud, and B. Maro. 1992. Cell cycle modification during the transitions between meiotic M-phases in mouse oocytes. *J Cell Sci*. 102 (Pt 3):457-467.

Kudo, N.R., K. Wassmann, M. Anger, M. Schuh, K.G. Wirth, H. Xu, W. Helmhart, H. Kudo, M. McKay, B. Maro, J. Ellenberg, P. de Boer, and K. Nasmyth. 2006. Resolution of chiasmata in oocytes requires separase-mediated proteolysis. *Cell*. 126:135-146.

Lane, S.I., Y. Yun, and K.T. Jones. 2012. Timing of anaphase-promoting complex activation in mouse oocytes is predicted by microtubule-kinetochore attachment but not by bivalent alignment or tension. *Development*. 139:1947-1955.

Ledan, E., Z. Polanski, M.E. Terret, and B. Maro. 2001. Meiotic maturation of the mouse oocyte requires an equilibrium between cyclin B synthesis and degradation. *Dev Biol*. 232:400-413.

Li, J., J.X. Tang, J.M. Cheng, B. Hu, Y.Q. Wang, B. Aalia, X.Y. Li, C. Jin, X.X. Wang, S.L. Deng, Y. Zhang, S.R. Chen, W.P. Qian, Q.Y. Sun, X.X. Huang, and Y.X. Liu. 2018a. Cyclin B2 can compensate for Cyclin B1 in oocyte meiosis I. *J Cell Biol*. 217:3901-3911.

Li, X.C., and J.C. Schimenti. 2007. Mouse pachytene checkpoint 2 (trip13) is required for completing meiotic recombination but not synapsis. *PLoS Genet*. 3:e130.

Li, Y., L. Wang, L. Zhang, Z. He, G. Feng, H. Sun, J. Wang, Z. Li, C. Liu, J. Han, J. Mao, X. Yuan, L. Jiang, Y. Zhang, Q. Zhou, and W. Li. 2018b. Cyclin B3 is specifically required for metaphase to anaphase transition in mouse oocyte meiosis I. *bioRxiv*. doi.org/10.1101/390351 (Preprint posted August 20, 2018)

Lischetti, T., and J. Nilsson. 2015. Regulation of mitotic progression by the spindle assembly checkpoint. *Mol Cell Oncol*. 2:e970484.

Lozano, J.C., V. Verge, P. Schatt, J.L. Juengel, and G. Peaucellier. 2012. Evolution of cyclin B3 shows an abrupt three-fold size increase, due to the extension of a single exon in placental mammals, allowing for new protein-protein interactions. *Mol Biol Evol*. 29:3855-3871.

Malumbres, M., E. Harlow, T. Hunt, T. Hunter, J.M. Lahti, G. Manning, D.O. Morgan, L.H. Tsai, and D.J. Wolgemuth. 2009. Cyclin-dependent kinases: a family portrait. *Nat Cell Biol*. 11:1275-1276.

Meijer, L., A. Borgne, O. Mulner, J.P. Chong, J.J. Blow, N. Inagaki, M. Inagaki, J.G. Delcros, and J.P. Moulinoux. 1997. Biochemical and cellular effects of roscovitine, a potent and selective inhibitor of the cyclin-dependent kinases cdc2, cdk2 and cdk5. *Eur J Biochem*. 243:527-536.

Miles, D.C., J.A. van den Bergen, A.H. Sinclair, and P.S. Western. 2010. Regulation of the female mouse germ cell cycle during entry into meiosis. *Cell cycle*. 9:408-418.

Morgan, D.O. 1997. Cyclin-dependent kinases: engines, clocks, and microprocessors. *Annu Rev Cell Dev Biol*. 13:261-291.

Nguyen, T.B., K. Manova, P. Capodieci, C. Lindon, S. Bottega, X.Y. Wang, J. Refik-Rogers, J. Pines, D.J. Wolgemuth, and A. Koff. 2002. Characterization and expression of mammalian cyclin b3, a prepachytene meiotic cyclin. *J Biol Chem*. 277:41960-41969.

Niault, T., K. Hached, R. Sotillo, P.K. Sorger, B. Maro, R. Benezra, and K. Wassmann. 2007. Changing Mad2 levels affects chromosome segregation and spindle assembly checkpoint control in female mouse meiosis I. *PLoS ONE*. 2:e1165.

Nieduszynski, C.A., J. Murray, and M. Carrington. 2002. Whole-genome analysis of animal A- and B-type cyclins. *Genome Biol*. 3:RESEARCH0070.

Nikalayevich, E., N. Bouftas, and K. Wassmann. 2018. Detection of Separase Activity Using a Cleavage Sensor in Live Mouse Oocytes. *Methods Mol Biol*. 1818:99-112.

Ortega, S., I. Prieto, J. Odajima, A. Martin, P. Dubus, R. Sotillo, J.L. Barbero, M. Malumbres, and M. Barbacid. 2003. Cyclin-dependent kinase 2 is essential for meiosis but not for mitotic cell division in mice. *Nat Genet*. 35:25-31.

Petronczki, M., M.F. Siomos, and K. Nasmyth. 2003. Un menage a quatre: the molecular biology of chromosome segregation in meiosis. *Cell*. 112:423-440.

Rattani, A., P.K. Vinod, J. Godwin, K. Tachibana-Konwalski, M. Wolna, M. Malumbres, B. Novak, and K. Nasmyth. 2014. Dependency of the spindle assembly checkpoint on Cdk1 renders the anaphase transition irreversible. *Curr Biol*. 24:630-637.

Refik-Rogers, J., K. Manova, and A. Koff. 2006. Misexpression of cyclin B3 leads to aberrant spermatogenesis. *Cell cycle*. 5:1966-1973.

Romanienko, P.J., J. Giacalone, J. Ingenito, Y. Wang, M. Isaka, T. Johnson, Y. You, and W.H. Mark. 2016. A vector with a single promoter for *in vitro* transcription and mammalian cell expression of CRISPR gRNAs. *PLoS One*. 11:e0148362.

Santaguida, S., A. Tighe, A.M. D'Alise, S.S. Taylor, and A. Musacchio. 2010. Dissecting the role of MPS1 in chromosome biorientation and the spindle checkpoint through the small molecule inhibitor reversine. *J Cell Biol*. 190:73-87.

Santamaria, D., C. Barriere, A. Cerqueira, S. Hunt, C. Tardy, K. Newton, J.F. Caceres, P. Dubus, M. Malumbres, and M. Barbacid. 2007. Cdk1 is sufficient to drive the mammalian cell cycle. *Nature*. 448:811-815.

Schulman, B.A., D.L. Lindstrom, and E. Harlow. 1998. Substrate recruitment to cyclin-dependent kinase 2 by a multipurpose docking site on cyclin A. *Proc Natl Acad Sci U S A*. 95:10453-10458.

Shindo, N., K. Kumada, and T. Hirota. 2012. Separase sensor reveals dual roles for separase coordinating cohesin cleavage and cdk1 inhibition. *Dev Cell*. 23:112-123.

Sigrist, S., H. Jacobs, R. Stratmann, and C.F. Lehner. 1995. Exit from mitosis is regulated by Drosophila fizzy and the sequential destruction of cyclins A, B and B3. *Embo J*. 14:4827-4838.

Stemmann, O., I.H. Gorr, and D. Boos. 2006. Anaphase topsy-turvy: Cdk1 a securin, separase a CKI. *Cell Cycle*. 5:11-13.

Stern, B., and P. Nurse. 1996. A quantitative model for the cdc2 control of S phase and mitosis in fission yeast. *Trends Genet*. 12:345-350.

Swaffer, M.P., A.W. Jones, H.R. Flynn, A.P. Snijders, and P. Nurse. 2016. CDK Substrate Phosphorylation and Ordering the Cell Cycle. *Cell*. 167:1750-1761 e1716.

Tang, J.X., D. Chen, S.L. Deng, J. Li, Y. Li, Z. Fu, X.X. Wang, Y. Zhang, S.R. Chen, and Y.X. Liu. 2018. CRISPR/Cas9-mediated genome editing induces gene knockdown by altering the pre-mRNA splicing in mice. *BMC Biotechnol*. 18:61.

Terret, M.E., K. Wassmann, I. Waizenegger, B. Maro, J.M. Peters, and M.H. Verlhac. 2003. The meiosis I-to-meiosis II transition in mouse oocytes requires separase activity. *Curr Biol*. 13:1797-1802.

Touati, S.A., E. Buffin, D. Cladiere, K. Hached, C. Rachez, J.M. van Deursen, and K. Wassmann. 2015. Mouse oocytes depend on BubR1 for proper chromosome segregation but not for prophase I arrest. *Nat Commun*. 6:6946.

Touati, S.A., D. Cladiere, L.M. Lister, I. Leontiou, J.P. Chambon, A. Rattani, F. Bottger, O. Stemmann, K. Nasmyth, M. Herbert, and K. Wassmann. 2012. Cyclin A2 Is Required for Sister Chromatid Segregation, But Not Separase Control, in Mouse Oocyte Meiosis. *Cell Rep*. 10.1016/j.celrep.2012.10.002

Touati, S.A., and K. Wassmann. 2016. How oocytes try to get it right: spindle checkpoint control in meiosis. *Chromosoma*. 125:321-335.

Treen, N., T. Heist, W. Wang, and M. Levine. 2018. Depletion of Maternal Cyclin B3 Contributes to Zygotic Genome Activation in the Ciona Embryo. *Curr Biol*. 28:1330-1331.

Tsurumi, C., S. Hoffmann, S. Geley, R. Graeser, and Z. Polanski. 2004. The spindle assembly checkpoint is not essential for CSF arrest of mouse oocytes. *J Cell Biol*. 167:1037-1050.

Uhlmann, F., C. Bouchoux, and S. Lopez-Aviles. 2011. A quantitative model for cyclin-dependent kinase control of the cell cycle: revisited. *Philos Trans R Soc Lond B Biol Sci*. 366:3572-3583.

van der Voet, M., M.A. Lorson, D.G. Srinivasan, K.L. Bennett, and S. van den Heuvel. 2009. C. elegans mitotic cyclins have distinct as well as overlapping functions in chromosome segregation. *Cell cycle*. 8:4091-4102.

Wassmann, K., and R. Benezra. 1998. Mad2 transiently associates with an APC/p55Cdc complex during mitosis. *Proc Natl Acad Sci U S A*. 95:11193-11198.

Wassmann, K., T. Niault, and B. Maro. 2003. Metaphase I arrest upon activation of the Mad2-dependent spindle checkpoint in mouse oocytes. *Curr Biol*. 13:1596-1608.

Yang, Y., C.R. Yang, S.J. Han, E.M. Daldello, A. Cho, J.P.S. Martins, G. Xia, and M. Conti. 2017. Maternal mRNAs with distinct 3' UTRs define the temporal pattern of Ccnb1 synthesis during mouse oocyte meiotic maturation. *Genes Dev*. 31:1302-1307.

Yuan, K., and P.H. O'Farrell. 2015. Cyclin B3 is a mitotic cyclin that promotes the metaphase-anaphase transition. *Curr Biol*. 25:811-816.

Zhang, Q.H., W.S. Yuen, D. Adhikari, J.A. Flegg, G. FitzHarris, M. Conti, P. Sicinski, I. Nabti, P. Marangos, and J. Carroll. 2017. Cyclin A2 modulates kinetochore-microtubule attachment in meiosis II. *J Cell Biol*. 216:3133-3143.

Zhang, T., S.T. Qi, L. Huang, X.S. Ma, Y.C. Ouyang, Y. Hou, W. Shen, H. Schatten, and Q.Y. Sun. 2015. Cyclin B3 controls anaphase onset independent of spindle assembly checkpoint in meiotic oocytes. *Cell Cycle*. 14:2648-2654.

Figure legends

Figure 1. Generation of *Ccnb3*$^{-/-}$ mice reveals a requirement for cyclin B3 in female meiosis.

(**A**) Targeted mutation of *Ccnb3*. (Top) Exons 6 and 7 are shown as black rectangles. A portion of the sequences of the wild-type allele and *em1* mutant allele are shown, with guide RNA position in red and the complement of the PAM sequence in blue. (Bottom) Schematic of cyclin B3 protein.

(**B**) Immunoprecipitation and western blot analysis of adult testis extracts using an anti-cyclin B3 monoclonal antibody.

(**C**) Apparently normal folliculogenesis and oocyte reserves in *Ccnb3*-deficient females. (Left) PFA-fixed, anti-MVH stained ovary sections from three-month-old animals. Zoomed images show presence of primary/primordial follicles indicated by black arrows. Scale bars: 200 µm. (Right) Oocyte counts from two three-month-old females of each genotype. PFA-fixed ovaries were sectioned completely and stained with anti-MVH. Stained oocytes were counted in every fifth ovary section and summed. Each point is the count for one ovary of one animal, means are 1114 for *Ccnb3*$^{+/-}$, and 987 for *Ccnb3*$^{-/-}$.

(**D**) The scheme illustrates progression through the meiotic divisions until metaphase II arrest in oocytes of the mouse strain used. The graph on the right shows percentages of mature oocytes of the indicated genotypes that underwent GVBD (germinal vesicle breakdown) within 90 min in culture after release, and oocytes that extruded polar bodies (PBs). n: total number of oocytes counted in more than 10 independent experiments (GVBD: 141 *Ccnb3*$^{+/-}$: 90.78 %; 119 *Ccnb3*$^{-/-}$: 89.91 %; PBE: 258 *Ccnb3*$^{+/-}$: 78.13 %; 342 *Ccnb3*$^{-/-}$: 9.06 %)

Figure 2. Cyclin B3 is required for the metaphase-to-anaphase I transition in oocytes.

(**A**) Live-cell imaging of meiotic maturation. β-tubulin-GFP and H2B-RFP mRNA to visualize spindle and chromosomes, were injected into GV-stage oocytes, which were then induced to enter meiosis I. Selected time frames are shown, with overlay of DIC, GFP and RFP channels of collapsed z-sections (11 section, 3-µm steps) from a representative movie. Time after GVBD is indicated as hours : minutes. n indicates number of oocytes analyzed. Percentage of oocytes of the observed phenotype from two independent experiments is indicated. Scale bar represents 20 µm, white asterisks indicate PBs. Related to Supplemental Movies 1 and 2.

(**B**) Chromosome spreads 6 hours (corresponding to metaphase I) and 16 hours (corresponding to metaphase II in controls) after GVBD. Kinetochores were stained with CREST (green), chromosomes with Hoechst (blue). Insets show typical chromosome figures observed; for better visualization chromosomes are shown in grayscale. Schematics of metaphase I bivalents or metaphase II univalent

chromosomes are shown to aid interpretation. Scale bar represents 5 μm; n: number of oocytes analyzed in three independent experiments.

(**C**) Whole-mount immunofluorescence staining of cold-treated spindles. Microtubules were stained with anti-tubulin antibody (green), kinetochores with CREST (red), and chromosomes with Hoechst (blue). Spindle poles typical of metaphase I and metaphase II are indicated with arrowhead in controls. Scale bar: 5 μm; n: number of oocytes analyzed in three independent experiments.

Figure 3. Cell cycle arrest in *Ccnb3*$^{-/-}$ oocytes is associated with incomplete APC/C activation.

(**A**) Schematic of the separase activity sensor. See text for details.

(**B**) Failure to activate separase in absence of cyclin B3. Separase activity sensor mRNA was injected into GV oocytes, which were released into meiosis I and visualized by spinning disk confocal microscopy. Selected time frames of collapsed z-sections (11 section, 3-μm steps) from a representative movie are shown. Time points after GVBD are indicated as hours : minutes. Scale bar: 20 μm; white asterisks indicate PBs; n: number of oocytes from three independent experiments.

(**C**) Western blot analysis of cyclin B1 and securin during oocyte maturation, at the time points indicated as hours : minutes after GVBD. β-actin serves as loading control. The number of oocytes used and the presence or absence of a PB are indicated. Two mice of each genotype were used per experiment. The data shown are representative of results from two independent experiments.

(**D**) Total cyclin B-CDK1 activity during oocyte maturation, at the time points indicated as hours : minutes after GVBD. Histone H1 was used as a substrate. Five oocytes were used per kinase reaction, presence or absence of a PB is indicated. The graph shows quantification of phosphate incorporation from three independent experiments and error bars indicate standard deviation (Mean +/- s.d.: lane 1: 100 (used for normalization); lane 2: 31.27 +/- 37.28; lane 3: 109.34 +/- 17.09; lane 4: 104.05 +/- 19.33; lane 5: 98.67 +/- 50.56; lane 6: 65.40 +/- 22.12)

(**E**) CDK inhibition rescues meiosis I division. Oocytes were incubated with SiR-DNA to visualize chromosomes. In metaphase I, 6 hours 20 minutes after GVBD, oocytes were treated with 0.2 mM roscovitine (final concentration), where indicated, and the movie was started. Selected time frames of collapsed z-sections (11 section, 3-μm steps) of DIC and far-red channel from a representative movie of *Ccnb3*$^{-/-}$ oocytes with or without roscovitine treatment are shown. The asterisk indicates chromosome segregation in anaphase I. Time points after GVBD are indicated as hours : minutes. Scale bar: 20 μm; n: number of oocytes from three independent experiments.

(**F**) Degradation of exogenous APC/C substrates. Securin-YFP (above) or cyclin B1-GFP (below) mRNA was injected into GV oocytes. Stills from representative movies are shown. Time points after GVBD are indicated as hours: minutes. Scale bar: 20 μm (n: number of oocytes from two independent experiments),

white asterisk indicates polar body extrusion (PBE). Fluorescence intensities (mean +/- s.d.) were quantified from the indicated number of oocytes imaged (securin-YFP: 4 *Ccnb3*$^{-/-}$, 6 *Ccnb3*$^{+/-}$, cyclin B1-GFP injections: 6 *Ccnb3*$^{-/-}$, 8 *Ccnb3*$^{+/-}$).

Figure 4. SAC activation is not the cause of metaphase I arrest in *Ccnb3*$^{-/-}$ oocytes.

(**A**) Left: Chromosome spreads were prepared 3 hours (early prometaphase I) and 6 hours (metaphase I) after GVBD, then stained with Hoechst (blue), CREST (green), and anti-MAD2 (red). Scale bar: 5 μm. Right: Quantification of MAD2 signal intensity relative to CREST; each point is the mean relative intensity averaged across centromeres in an oocyte. n: number of oocytes from three independent experiments. P values are from t tests (n.s., not significant). Number and means of oocytes stained 3 hours after GVBD: 23 *Ccnb3*$^{+/-}$ (mean: 0.794) 19 *Ccnb3*$^{-/-}$ (mean: 0.77), 6 hours after GVBD: 26 *Ccnb3*$^{+/-}$ (mean: 0.302), and 20 *Ccnb3*$^{-/-}$ (mean: 0.325).

(**B**) Oocytes were treated with reversine to override a potential SAC arrest. Control oocytes were treated with nocodazole from 6 hours after GVBD onwards, whereas *Ccnb3*$^{-/-}$ oocytes were allowed to arrest without nocodazole. 6 hours 40 min after GVBD, reversine was added, PB extrusion was scored visually (graph on the right, n: number of oocytes scored per genotype. 0 % of oocytes extruded PBs, except oocytes treated with nocodazole and reversine, which extruded PBs in 85.29 % of oocytes analyzed), and all oocytes were spread 20 hours after GVBD. Kinetochores were stained with CREST (green) and chromosomes with Hoechst (blue). Insets show typical chromosome figures observed. Scale bar: 5 μm; n indicates the number of spreads from three independent experiments that allowed to unambigiously distinguish bivalents from univalents, percentage of oocytes with same phenotype is indicated.

Figure 5. Ordered degradation of APC/C substrates in oocyte meiosis I.

(**A,B**) Cyclin B3 is degraded after securin or cyclin A2. mRNA encoding cyclin B3-RFP and either securin-YFP (panel A, 20 oocytes) or cyclin A2-GFP (panel B, 19 oocytes) were co-injected into GV oocytes of CD-1 mice. Each panel shows selected frames from a movie of a representative oocyte, with an overlay of DIC and RFP channels in the top rows, and DIC and YFP or GFP channels in the bottom rows.

(**C**) The D box of cyclin B3 is required for degradation. CD-1 GV oocytes (10 oocytes) were injected with mRNA encoding cyclin B3-RFP with the D box deleted (ΔDbox). Frames from a representative movie are shown, with the DIC channel on top and RFP at the bottom.

All panels: Time points after GVBD (BD) are indicated as hours : minutes; scale bars: 20 μm; white asterisks: PBs. Quantification of fluorescence intensities is shown on the right (mean +/- s.d. of the indicated number of oocytes from three independent experiments).

Figure 6. Only cyclin B3 that can support *in vitro* kinase activity can rescue *Ccnb3*$^{-/-}$ oocytes.

(**A**) Affinity purification of cyclin B3-CDK1 complexes. ^{MBPHis}cyclin B3 or ^{MBPHis}cyclin B3 MRL mutant were expressed in insect cells alone or co-expressed with either untagged or HA-tagged CDK1. (Left) The eluates from purification on amylose resin were separated on SDS-PAGE and stained with Coomasssie. (Right) Representative autoradiograph (top) and quantification (bottom) from histone H1 kinase assays. In the graph, values in each experiment (n = 3) were normalized to the signal from the ^{MBPHis}cyclin B3 MRL sample (lane 4 in the autoradiograph), lines indicate means (lane 1: 1.733; lane 2: 4.351; lane 3: 3.878; lane 4: 0 (used for normalization); lane 5: 0.121; lane 6: -0.202).

(**B**) Rescue of *Ccnb3*$^{-/-}$ oocytes by expression of exogenous cyclin B3. *Ccnb3*$^{-/-}$ oocytes were sham-injected or injected with the indicated cyclin mRNA, then released into meiosis I. Frames of representative movies are shown. Times after GVBD are indicated as hours : minutes and percentages of oocytes of the shown phenotypes are indicated. Scale bar: 20 μm; white asterisks: PBs; n: number of oocytes from three independent experiments.

(C) Total cyclin B-CDK1 activity during oocyte maturation, in control (lane 1-3), and *Ccnb3*$^{-/-}$ (lanes 4–9, labelled in red) oocytes expressing wild-type cyclin B3 (lanes 6 and 7) or ΔDbox cyclin B3 (lanes 8 and 9), at the time points indicated as hours : minutes after GVBD. Oocytes extruding PBs are indicated. Histone H1 was used as a substrate. A representative example from two independent experiments is shown above; quantification of both experiments is shown below (^{32}P-H1 signal normalized to the signal in lane 2; points are values from each experiment, lines indicate means: lane 1: 6.61; lane 2: 100 (used for normalization); lane 3: 14.38; lane 4: 191.58; lane 5: 138.53; lane 6: 109.88; lane 7: 9.59; lane 8: 37.36; lane 9: 1.5).

(**D**) Representative chromosome spreads 16 hours after GVBD. In the case of oocytes injected with the wild type cyclin B3 construct, only oocytes that had extruded PBs were analyzed. Chromosomes were stained with Hoechst (blue) and kinetochores with CREST (green). Insets show typical chromosome figures observed (chromosomes are shown in grayscale); scale bar: 5 μm; n: number of oocytes from three independent experiments. Schematics of metaphase I bivalents or metaphase II univalent chromosomes are shown to aid interpretation.

Figure 7. Inter-species cross-complementation of *Ccnb3*$^{-/-}$ oocytes.

(**A**) *Ccnb3*$^{-/-}$ oocytes were injected with the indicated mRNA, induced to enter meiosis I, and scored for PB extrusion. n: number of oocytes from three independent experiments, Number of oocytes analyzed and percentage of PB extrusion: 46 *Ccnb3*$^{-/-}$ sham injected oocytes (0 % PBs), 48 *Ccnb3*$^{-/-}$ oocytes injected with mRNA coding for *X. laevis* cyclin B3 (85.41 %), 20 *Ccnb3*$^{-/-}$ oocytes with *D. rerio* cyclin B3 mRNA (60 %), and 53 *Ccnb3*$^{-/-}$ oocytes with *D. melanogaster* cyclin B3 mRNA (92.45 %).

(**B**) Selected time frames of collapsed z-sections (12 sections, 3-µm steps) from a representative spinning disk confocal movie of *Ccnb3*$^{-/-}$ sham-injected oocytes, and *Ccnb3*$^{-/-}$ oocytes injected with *X. laevis* cyclin B3 mRNA. Prior to live imaging oocytes were incubated with SiR-DNA. Top panel shows the DIC channel and bottom panel shows SiR-DNA staining in far-red. Time points after GVBD are indicated as hours : minutes. Scale bar: 20 µm, white asterisks: PBs; n: number of oocytes from three independent experiments.

Supplemental Material

Supplemental Movie legends

Movie 1. Progression through meiosis I in control oocyte

A *Ccnb3*$^{+/-}$ oocyte incubated with SiR-DNA to visualize chromosomes. Acquisitions were started at GVBD + 6:30 (hours : minutes). Eleven z-sections with 3 μm steps were taken to follow chromosome movements, and shown are overlays of the stack. Acquisitions of the far-red and DIC channel were done every 20 min, 21 time points are shown. Related to Figure 2A. This is a representative movie from 42 oocytes from six independent experiments.

Movie 2. Progression through meiosis I in *Ccnb3*$^{-/-}$ oocyte

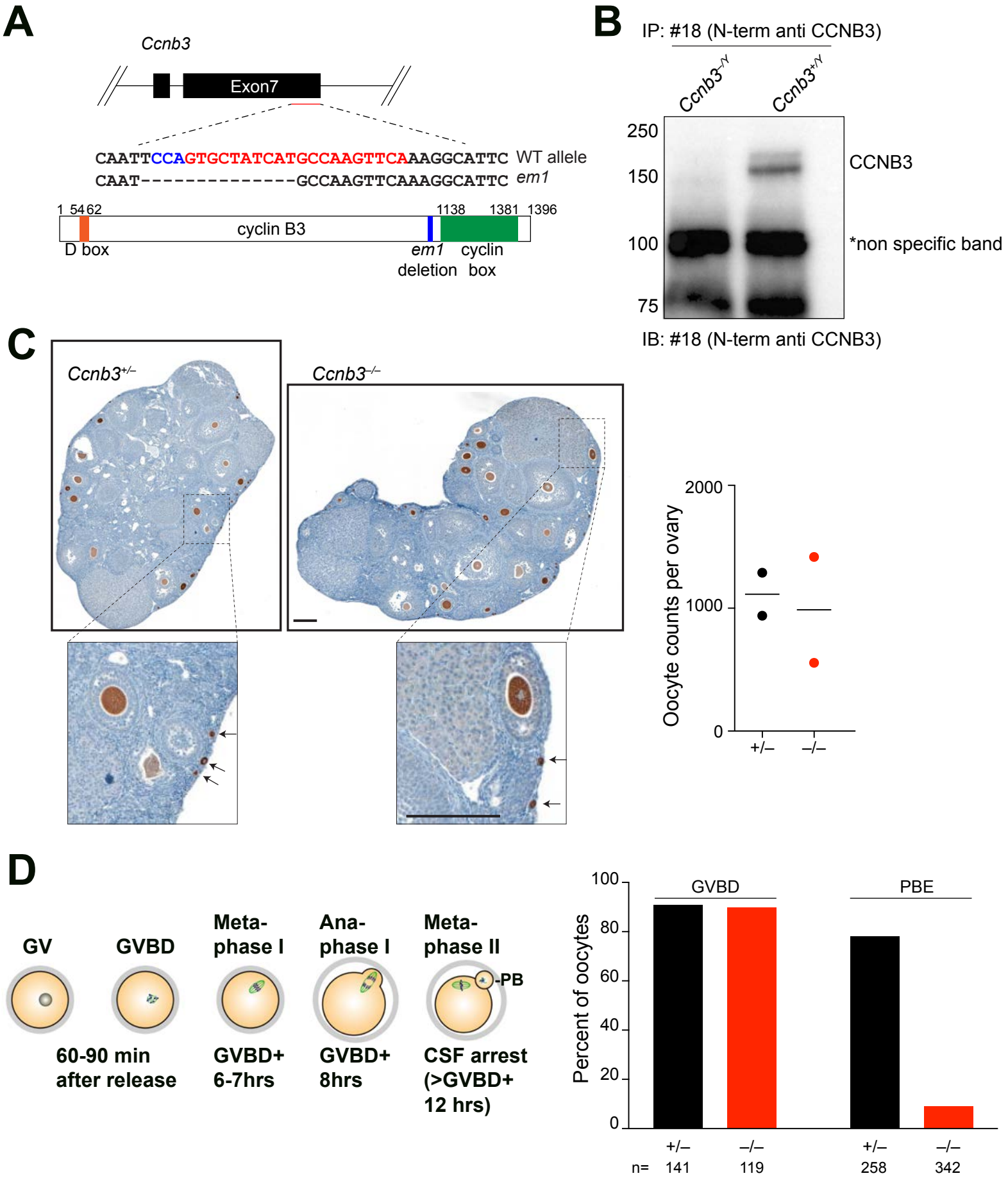
A *Ccnb3*$^{-/-}$ oocyte incubated with SiR-DNA to visualize chromosomes. Acquisitions were started at GVBD + 6:30 (hours : minutes). Eleven z-sections with 3 μm steps were taken to follow chromosome movements, and shown are overlays of the stack. Acquisitions of the far-red and DIC channel were done every 20 min, 21 time points are shown. Related to Figure 2A. This is a representative movie from 63 oocytes from six independent experiments.

Supplemental table legend

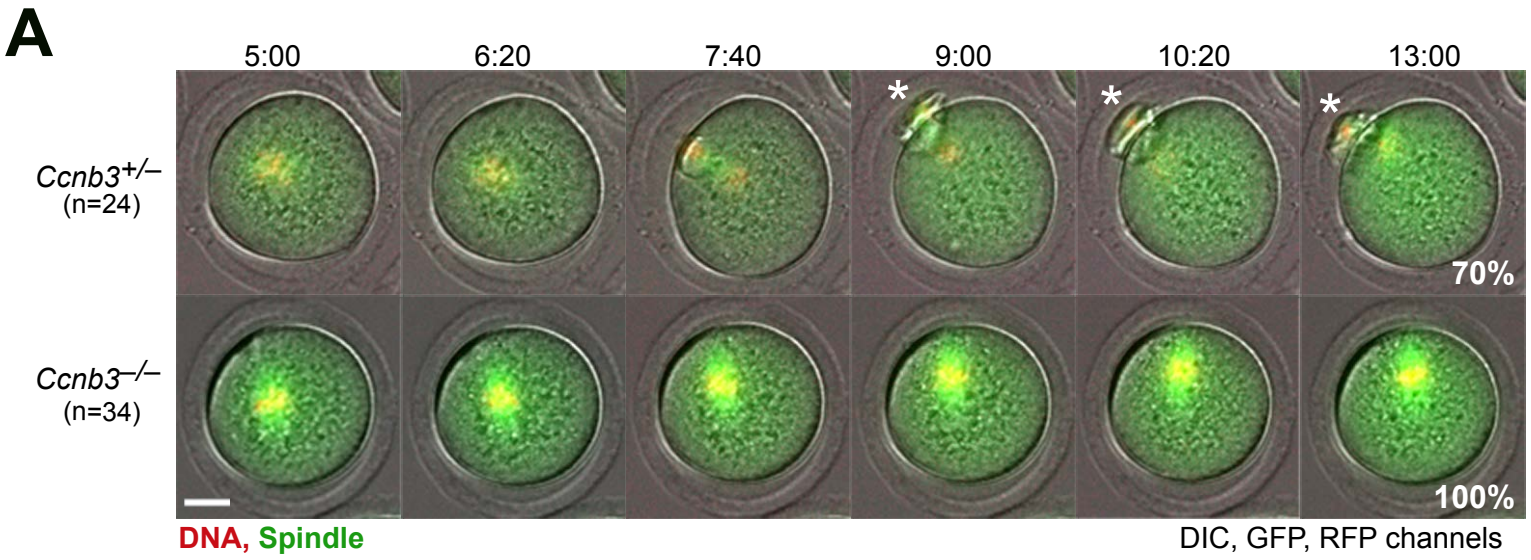
Table S1. Primers used for cloning expression plasmids

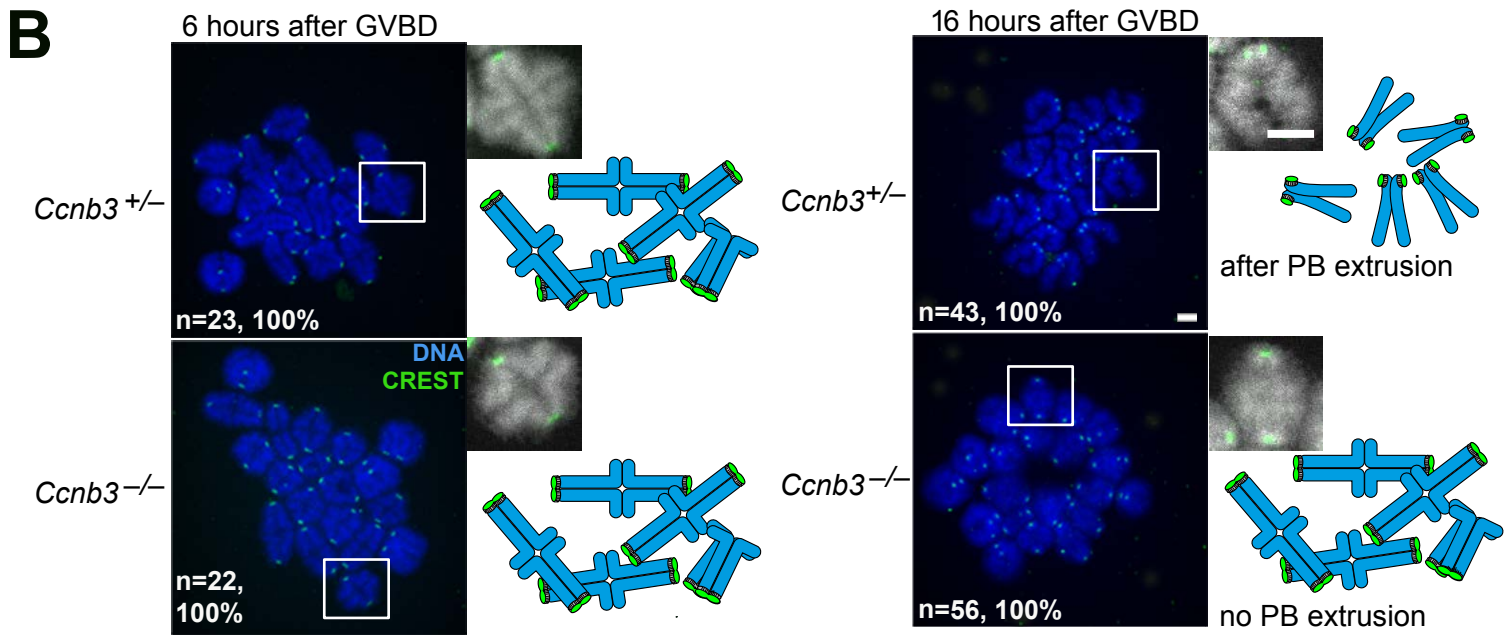
Primers used to generate the indicated plasmids are shown. See Methods section for details.

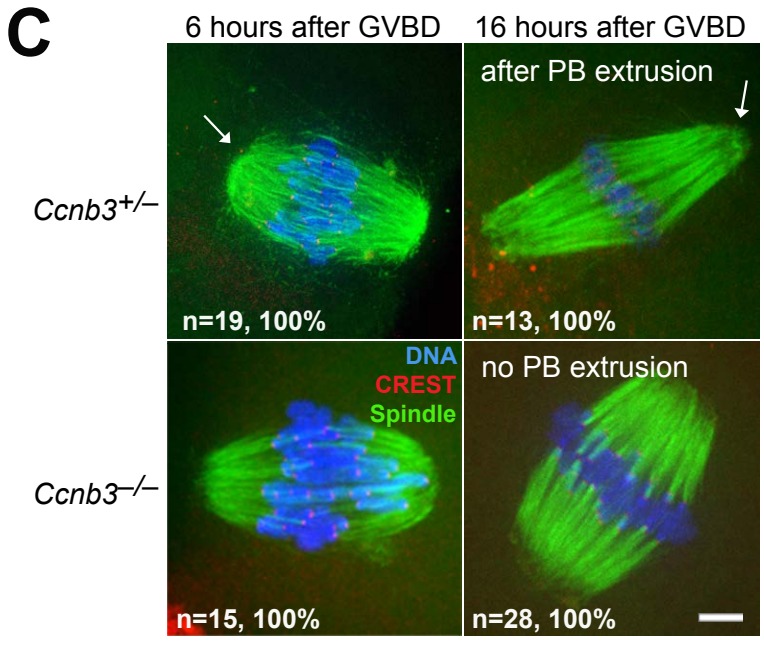
Karasu, Bouftas et al.,
Figure 1



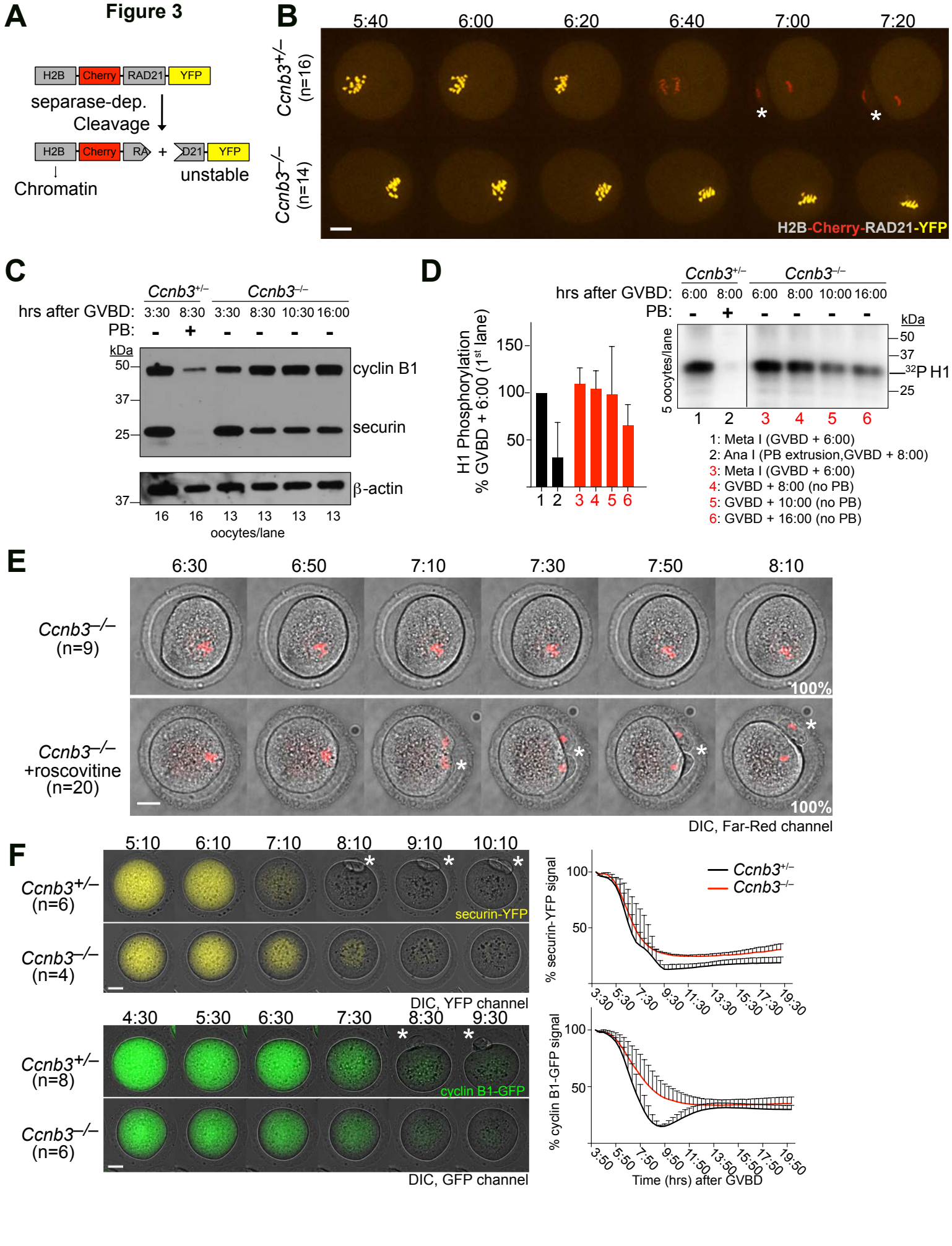
Karasu, Bouftas et al.,
Figure 2



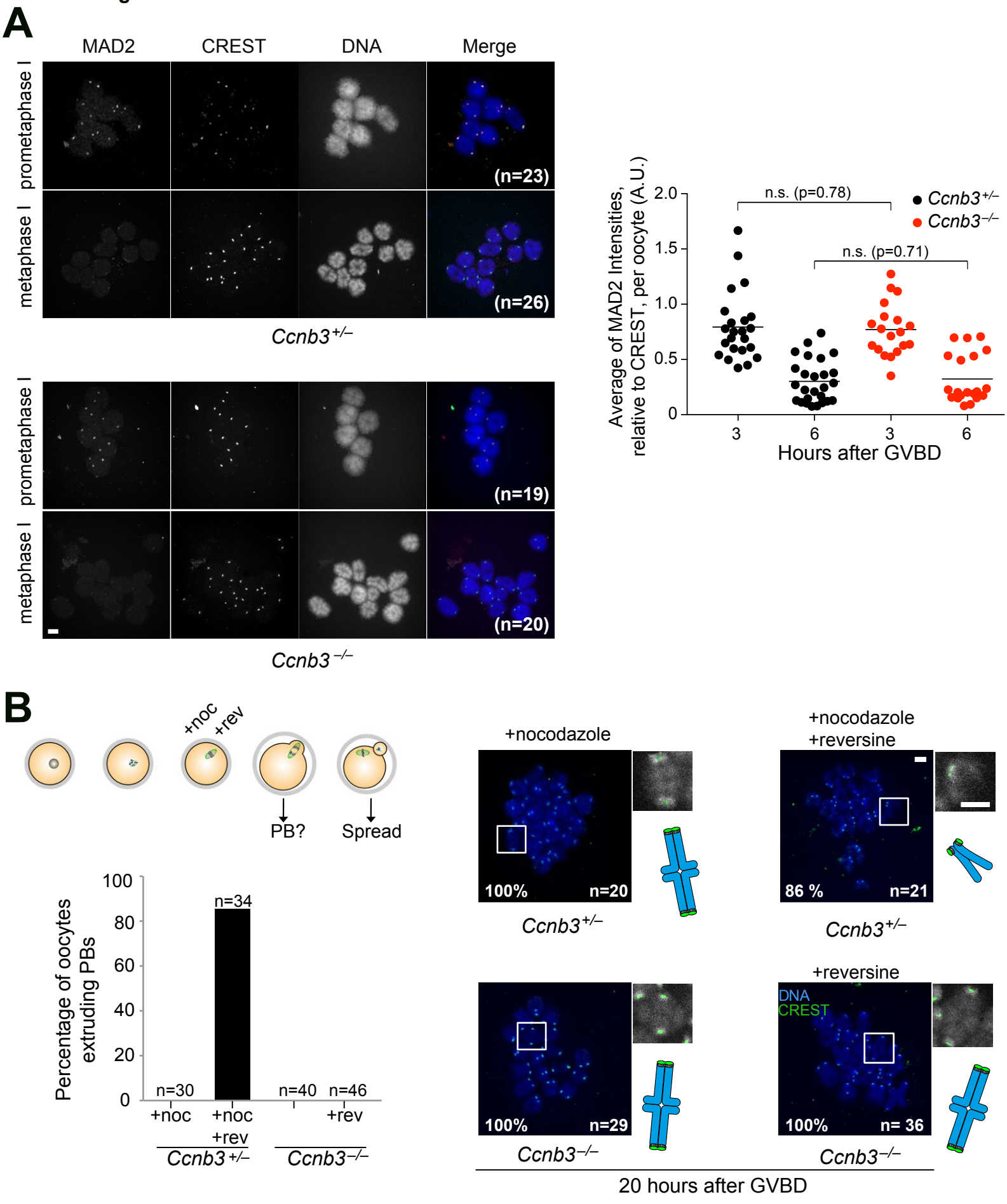




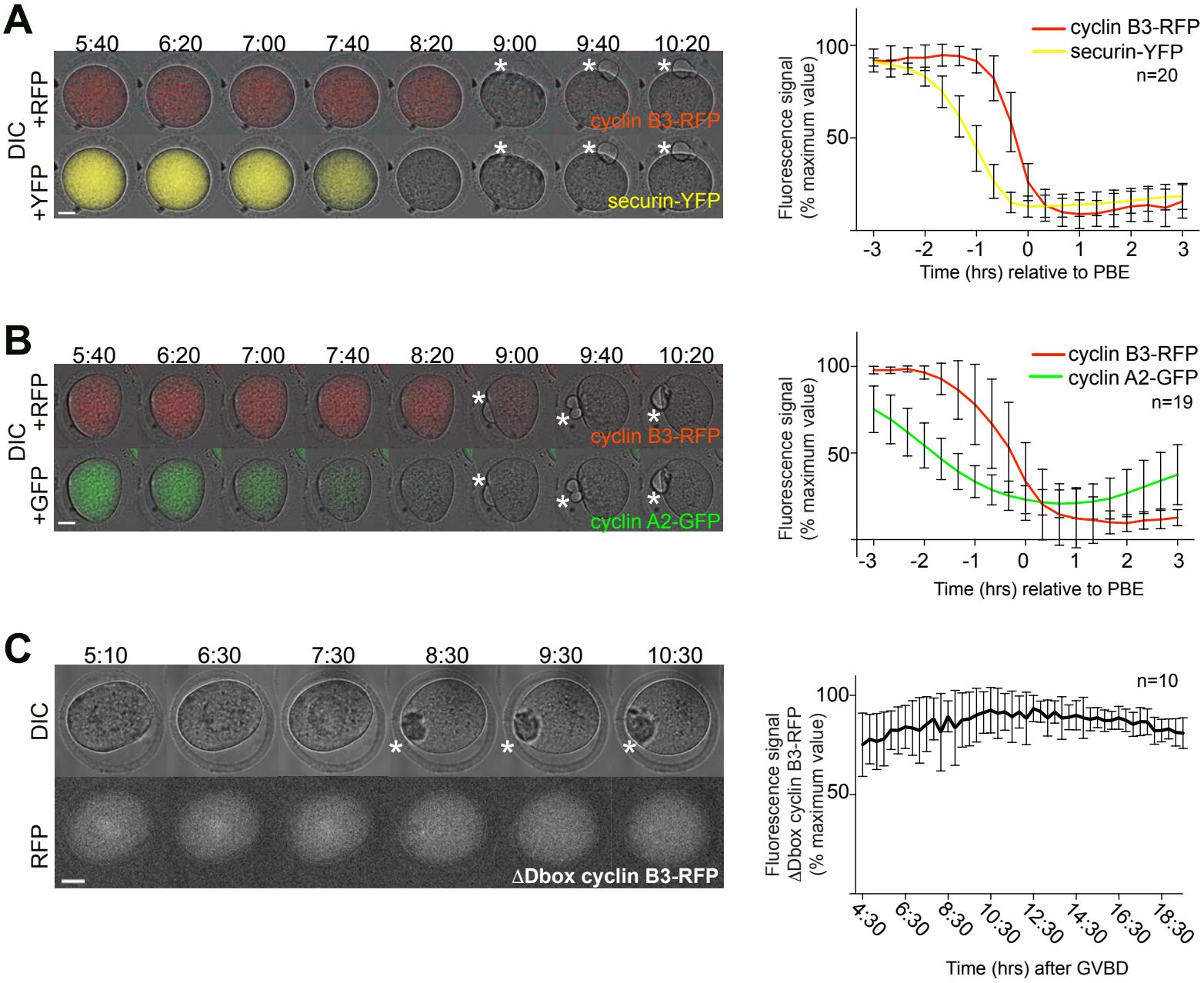
Karasu, Bouftas et al.,
Figure 3



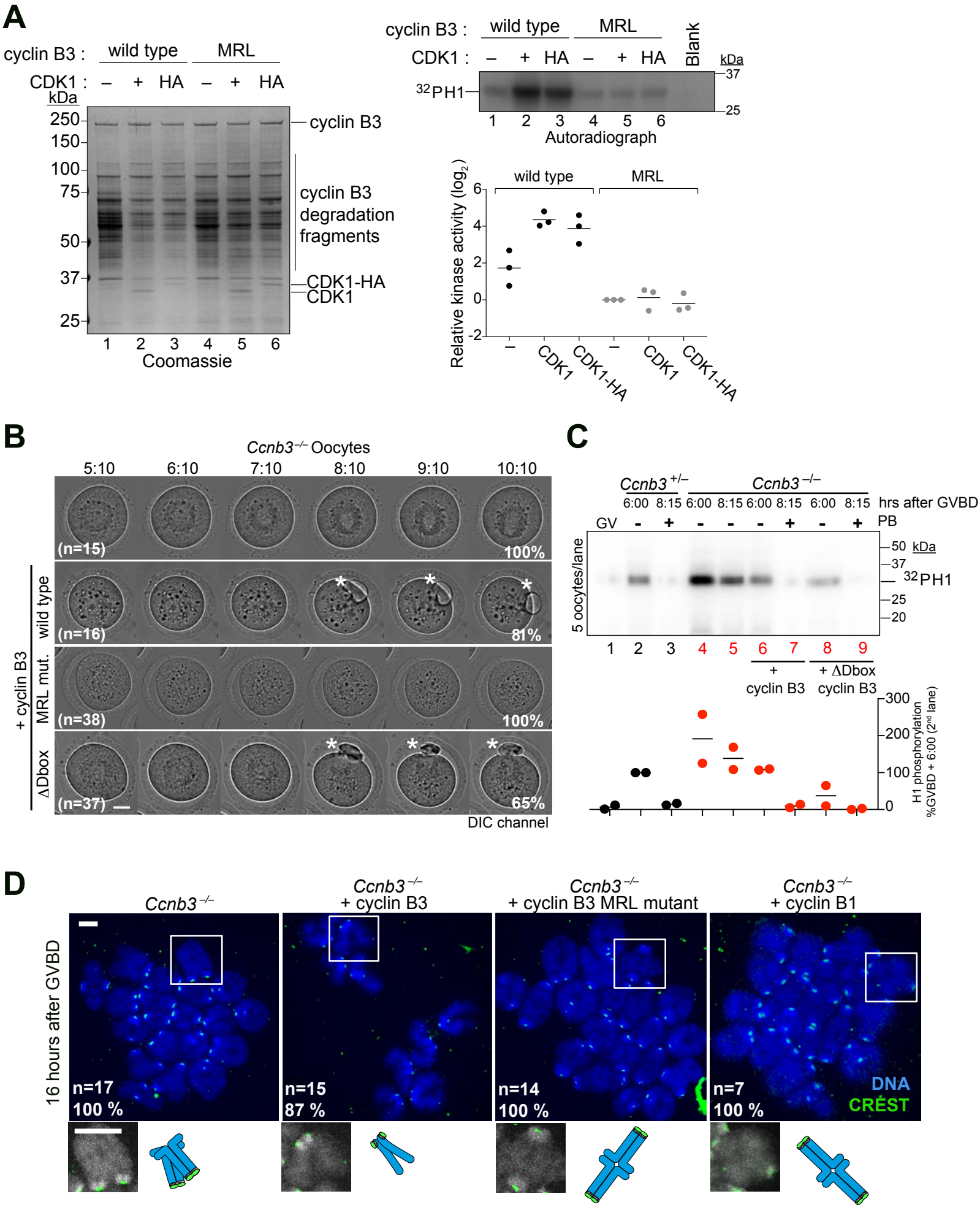
Karasu, Bouftas et al.,
Figure 4



Karasu, Bouftas et al.,
Figure 5



Karasu, Bouftas et al., Figure 6



Karasu, Bouftas et al.,
Figure 7

